DYNAMIC BEHAVIOR AND CHARACTERIZATION OF AUTOMOBILE CATALYSTS

Shinichi Matsumoto[1,*] and Hirofumi Shinjoh[2]

[1]**Toyota Motor Corporation, Material Engineering Div.1; 1 Toyota-cho, Toyota, Aichi, 471-8572 Japan**

[2]**Toyota Central R&D Labs., Inc., Nagakute, Aichi, 480-1192 Japan**

*Corresponding author. Tel.: +81-565-72-0213, +81-55-997-0501; Fax: +81-565-72-6887, +81-55-997-7879. E-mail: matumoto@shinichi.tec.toyota.co.jp

Advances in Chemical Engineering, vol. 33
ISSN 0065-2377
DOI 10.1016/S0065-2377(07)33001-9

Abstract

Automotive catalyst technology is now faced with very difficult problems. The recent progress of research on the dynamic behavior and characterization of automobile catalysts, and their development to solve these problems are reviewed in this chapter. The oxygen storage and release phenomena under the non-steady atmosphere are investigated in terms of the oxygen storage capacity, the oxygen mobility and the local structure of oxygen storage materials. These parameters are in good correlation with each other. The sintering and re-dispersion phenomena of Platinum Group Metals (PGM) on metal oxides are studied by X-ray absorption analysis. The sintering of Pt is suppressed by making a bond between Pt and surface oxygen of oxides such as CeO_2 under the oxygen rich atmosphere, and sintered Pt particles on CeO_2 are re-dispersed under appropriate conditions. The NO_x storage-reduction (NSR) catalyst, which was developed for automotive lean-burn engines, can reduce NO_x under the oxygen-rich atmosphere. The NO_x reduction phenomena are investigated by four steps. NO is oxidized on Pt under the oxygen-rich atmosphere. NO_2 reacts with basic materials and then is stored in the NSR as nitrate. The stored NO_x is released after the decomposition of nitrate under the oxygen deficient atmosphere. The released NO_x is reduced into N_2 on PGM by the reaction with a reducing component such as HC, CO and H_2. The main cause of deterioration for the NSR is sulfur poisoning. The sulfur-poisoning mechanism and the way for an NSR with high tolerance to sulfur poisoning is studied in storage materials, support materials, substrate structures and the arrangement of catalysts.

I. Introduction

Nowadays automobile prevails across the globe as the most popular and important mode of transportation in our daily life. About 50 million cars are produced each year, and totally over 700 million cars are being used worldwide. Thus, the application of automotive catalysts for detoxifying the pollutants, such as carbon monoxide (CO), hydrocarbons (HC), nitrogen oxides (NO_x) and particulate matter (PM) in the exhaust gases is absolutely indispensable in every vehicle.

The composition, temperature and flow amount of automotive exhaust gases vary continuously with driving conditions. The circumstance of the exhaust catalysts exposed is far more different from that in chemical factories. The automotive catalysts are requested to purify infinitesimally small amount of the

toxic gases in the exhaust perfectly under the unsteady condition, and also have a long-term durability during an automobile life. It is very important to manage and control the exhaust gas transient, in particular the fluctuation of atmosphere. The technology of automotive catalysts had already developed for the practical application, while it still needs to be paid more efforts for reaching the final goal of zero-emission.

In this chapter, following a general illustration on the automotive exhaust catalyst, we tried to discuss the recent progress and catalyst development for controlling the atmosphere fluctuation in the exhaust gases based on our research results.

II. Automotive Exhaust Catalyst and its Specific Features

A. Introduction of Exhaust Catalyst

In early 1970s, the serious photochemical smog in California brought the strict regulations of automotive exhaust emissions to both USA and Japan. Through lots of trials including engine modifications, the catalytic system for exhaust gases had been recognized as the only efficient method to meet the regulations. The oxidation catalyst for CO and HC was first adopted in 1974, and then in 1977, the 3-way catalyst (TWC) with the oxygen sensor was introduced for simultaneously detoxifying the three pollutant gases, CO, HC and NO_x. The catalytic methods for exhaust gases have established and most of automobiles have equipped the catalysts for emission control from then on.

The composition, temperature and flow amount of the exhaust gases from automobiles are very variable with the driving conditions. Figure 1 exemplifies an exhaust gas composition emitted from a gasoline engine as a function of air to fuel ratio (A/F) (Kummer, 1980). Much CO and HC are emitted under the rich condition, and there appears a NO_x emission peak around $A/F = 16$. The temperature of the catalyst ranges from sub-zero to more than 1,000°C, and the flow rate varies at different order of magnitude. The exhaust catalyst is requested to purify these toxic gases over such a wide range of these gas conditions as earlier.

Figure 2 illustrates a conventional monolith-type catalyst. Exhaust catalysts are composed of several components, including noble metals, Pt, Rh and Pd as active site, alumina-based supports with a high surface area even at high temperature, and metal oxides as promoter materials. Cerium oxides as oxygen storage material and basic materials for NO_x storage are typical promoter materials in the catalysts. The catalysts component is some hundreds micrometers thick and loaded on the substrate, usually made from cordielite ($2MgO_2 \cdot Al_2O_3 \cdot 5SiO_2$).

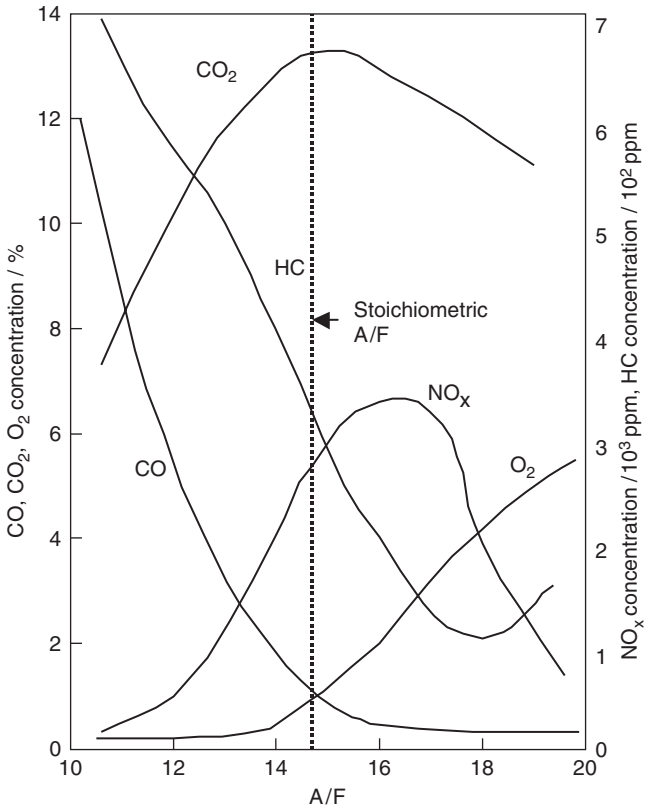

FIG. 1. Concentrations of CO, NO_x, HC (as hexane), O_2 and CO_2 emitted by spark-ignited engine as a function of the intake A/F.

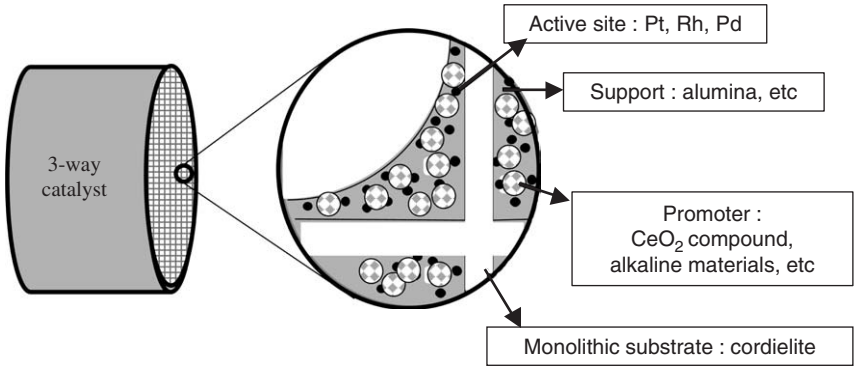

FIG. 2. Outline of 3-way catalyst.

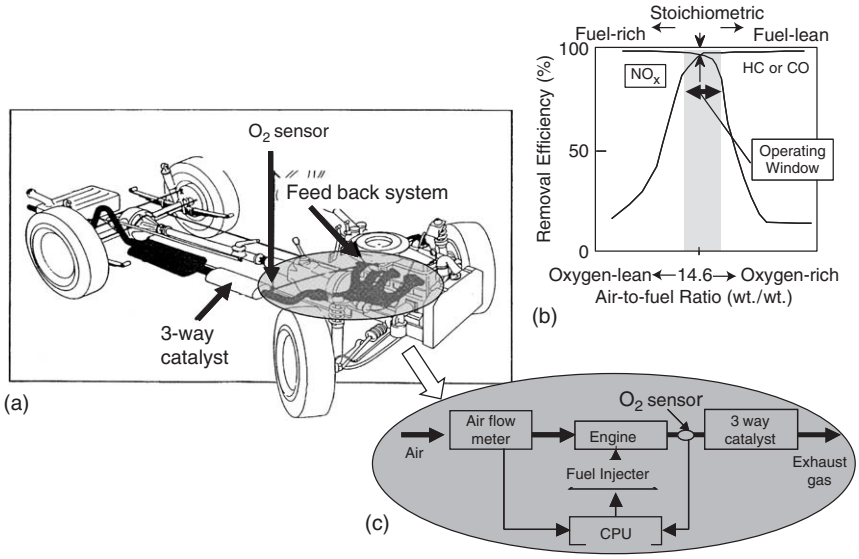

FIG. 3. 3-way catalyst system. (a) Diagram; (b) performance and (c) feedback system.

Figure 3 shows a TWC system and a typical performance of the TWC. The three components are highly purified over the catalyst around the stoichiometric point. The oxidizing and reducing components have almost the same chemical equivalent in the narrow shadowed region, and CO, HC and NO_x are converted into H_2O, CO_2 and N_2 (Fig. 3b). The atmosphere of the TWC is automatically controlled around the stoichiometric point by the TWC system. The flow rate of air is monitored and the fuel injection is controlled by a computerized system to obtain a suitable A/F ratio (Fig. 3c). The signal from oxygen sensor is used as a feedback for the fuel and air injection control loop. Therefore, the exhaust gases are fluctuating streams between oxidizing and reducing periodically and alternatively.

B. Catalytic Performance in Fluctuating Condition

The oscillations of atmosphere fluctuation occur with a frequency in the order of 1 Hz, and the catalytic activities are greatly affected by the species of noble metals and exhaust gas conditions. Figure 4 shows the NO_x conversion efficiency on a Pd catalyst as a function of oscillating periods and amplitudes in an engine test (Yokota *et al.*, 1985). This figure indicates that there are suitable cycling conditions, which the catalytic activities are superior to that under the static condition, and the catalyst performance depends on the cycling

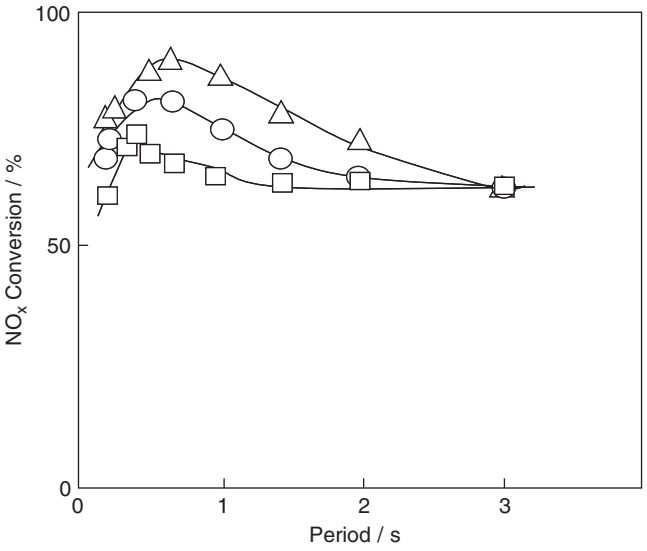

FIG. 4. NO_x reduction behavior on Pd/alumina catalyst as a function of oscillation periods and amplitudes in an engine test. Engine: 2 L, 1,600 rpm and −440 Torr; catalyst: Pd 0.05 g/L. A/F amplitude of oscillation: 0.4(△), 0.7(○) and 1.0(□).

conditions. These behaviors also found in the simulated exhaust gases and even in the simple binary reaction gas system such as $CO–O_2$, and Pd and Pt catalysts are particularly improved by controlling the cycling characteristics. Figure 5 illustrates an example of the periodic operation effect on simple binary gas systems (Muraki *et al.*, 1985). This figure shows the periodic operation effect for Pt catalyst in C_3H_6 oxidation (Shinjoh *et al.*, 1989). The maximum conversions are observed for any temperature, and the optimum period for maximum conversion decreases with increasing temperature. From the results of kinetics and evolution pattern analysis, the periodic operation effects arise from a difference of adsorption capability between the two reactants on the catalyst surface, that is, the self-poisoning reactant is the one more strongly adsorbed on the catalyst surface (Shinjoh *et al.*, 1987). Accordingly, the catalyst surface under static conditions is almost covered by the stronger ad-species, and the desired reactions are suppressed. Conversely, under optimum cycling conditions, these ad-species are eliminated and surface compositions are suitable for reaction to take place. Under these circumstances, the reaction rate reaches the maximum value. These periodic operation effects can be applied to improve the reactivity of TWCs by a selection of suitable cycling condition. Figure 6 shows CO oxidation reaction with various oscillation periods. The dashed line indicates the best operation for high CO conversion, that is, the oscillation period should be longer at low temperature (20 s at 50°C), and turns shorter

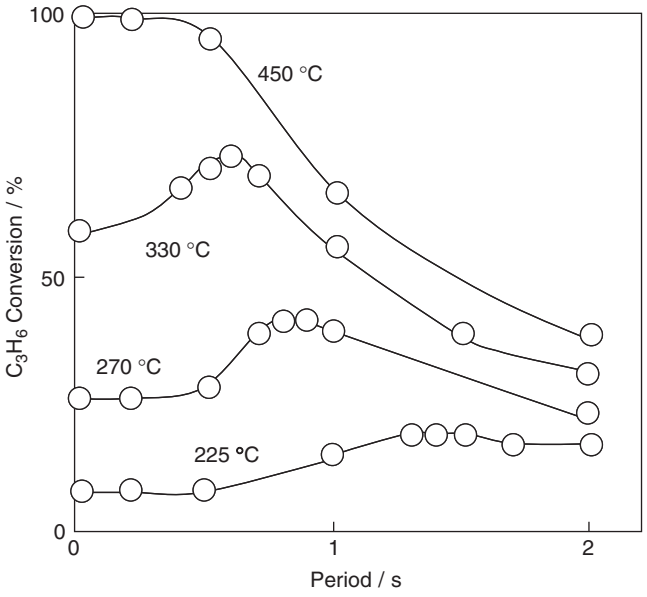

FIG. 5. Periodic operation effect on Pt/Al_2O_3 catalyst in C_3H_6–O_2 reaction.

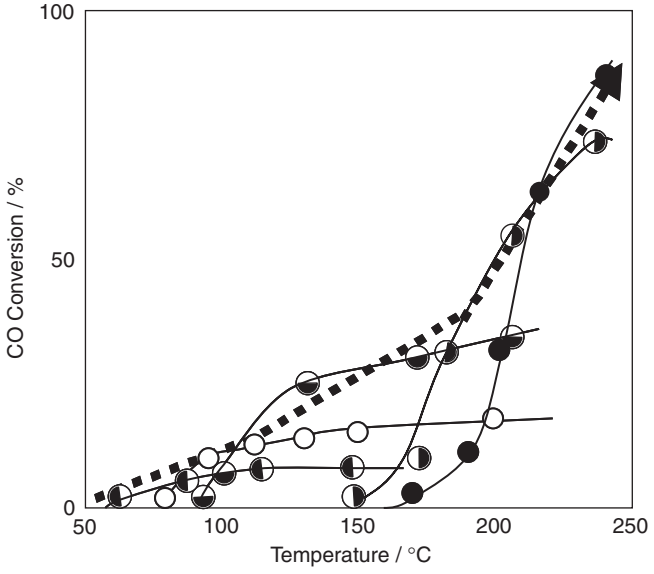

FIG. 6. Periodic operation effect on Pd/Al_2O_3 catalyst in CO–O_2 reaction. Oscillation periods: 0 s(●), 1 s(◑), 5 s(◒), 10 s(○) and 20 s(◐). Periodic operation effect on Pd/Al_2O_3 catalyst in CO–O_2 reaction.

with increasing temperature (10 s at 100°C, 5 s at 150°C and 1 s at 200°C), and keep a static condition at high temperature. However, these controls must be very difficult because exhaust gas conditions are changeable by individual driving mode and catalysts also change, which means catalyst degradation, with time. However, Rh catalysts show generally high catalytic performance with static condition. Rh is a requisite component for exhaust catalyst for its high NO_x reduction activity into N_2. Therefore, the other way to improve catalytic activity, in the opposite direction, is reducing the fluctuation by addition of oxygen storage materials as cerium compounds to the catalysts. These materials keep a stoichiometric atmosphere widely by adsorbing excess oxygen in oxidizing atmosphere, and releasing oxygen in reducing atmosphere. The oxygen storage materials are going to be discussed in the next chapter in more detail.

As the atmosphere fluctuation is one of the characteristic features for exhaust gases, it is very important for automotive use to optimize the catalysts under these conditions. One way is to overcome the demerit of these conditions for decreasing fluctuation, the other way is to utilize this operation in a positive manner. In this chapter, the way and the material for this purpose in automotive catalyst use was introduced as following: (1) oxygen storage material and its improvement, (2) Pt sintering and re-dispersion, (3) NO_x storage and reduction catalyst and NO_x reduction mechanism and (4) improvement on NO_x storage-reduction (NSR) catalyst system.

III. Oxygen Storage and Release in TWC

A. Introduction

TWCs have been continuously developed to improve their performance and durability since commercialized in 1977. The performance of TWCs is maximized in exhaust gas conditions close to the stoichiometric point. That is, the normal 14.5:1 (stoichiometric) ratio produces exhaust gas that contains the right balance of CO, H_2 and HC to reduce NO_x and O_2. CO, H_2 and HC are oxidized and NO_x and O_2 are reduced simultaneously into harmless CO_2, H_2O and N_2 on a TWC. However, the air–fuel ratio occasionally fluctuates in actual vehicle-driving conditions. In an actual vehicle driving in the LA#4 mode test, for example, NO_x emission increases during acceleration when the air–fuel ratio fluctuates out of the stoichiometic ratio (Fig. 7). To moderate the fluctuating atmosphere experienced by catalysts, materials with oxygen storage capacity (OSC) such as CeO_2 have been used in conventional TWCs (Gandhi *et al.*, 1976; Nagai *et al.*, 2002; Ozawa *et al.*, 1993). CeO_2 releases oxygen in an oxygen deficient atmosphere, and stores oxygen in an oxygen excess atmosphere as

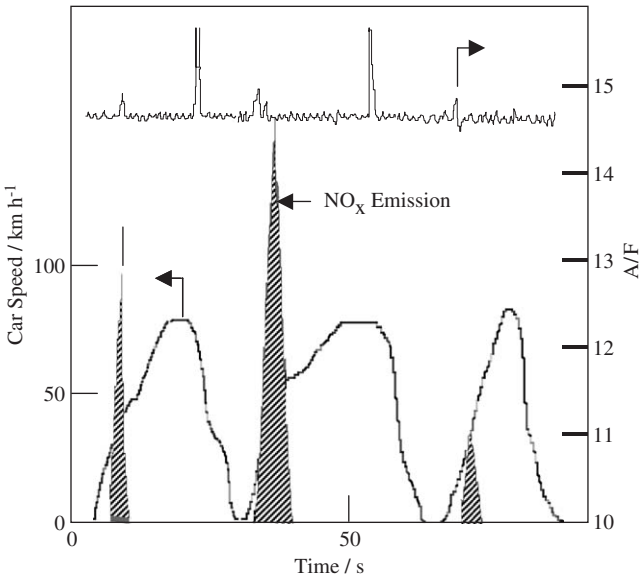

FIG. 7. Fluctuation of the air-fuel (A/F) ratio (solid line) and NO_x emissions (hatched line) of a vehicle in the LA#4 driving mode (dotted line).

described by the following reversible reaction:

$$CeO_2 \rightarrow CeO_{2(1-x)} + xO_2 \tag{1}$$

under the oxygen excess atmosphere, and

$$CeO_{2(1-x)} + xO_2 \rightarrow CeO_2 \tag{2}$$

under the oxygen deficient atmosphere, where $0 \leqslant x \leqslant 0.25$.

CeO_2 had been used in TWCs, but the thermal stability of pure CeO_2 is insufficient to meet the new requirements for low-emission vehicles. The investigations on the mechanism of the oxygen storage phenomena to develop a new oxygen storage material with high thermal stability are described in this chapter.

B. OSC OF MIXED OXIDE: $(Ce,La)O_{2-x}$, $(Ce,Zr)O_2$

Complex oxides of ceria were formed by pyrolysis of mixed precipitation from aqueous solution. Table I shows the XRD results of Ce–La and Ce–Zr mixed oxides calcined at 1,000°C (Matsumoto *et al.*, 1991). These results

TABLE I
PHASES FORMED IN CeO_2–La_2O_3 AND CeO_2–ZrO_2 SYSTEMS (MEASURED BY XRD)

x	Phase	x	Phase
$(Ce_{1-x},La_x)O_{2-x/2}$		$(Ce_{1-x},Zr_x)O_2$	
0	CeO_2	0	CeO_2
0.1	CeO_2 s.s.	0.1	CeO_2 s.s.
0.2	CeO_2 s.s.	0.2	CeO_2 s.s.
0.3	CeO_2 s.s. + C1	0.3	CeO_2 s.s. + C2
0.5	CeO_2 s.s. + La_2O_3 + C1	0.4	CeO_2 s.s. + ZrO_2 s.s. + C2

Note: s.s., solid solution with La or Zr oxide; C1 and C2, cubic fluorite-type oxide.

indicate the formation of solid solution $(Ce_{1-x},La_x)O_{2-x/2}$, complex oxides and La_2O_3 in the CeO_2–La_2O_3 system, and the formation of solid solution $(Ce_{1-x},Zr_x)O_2$ ($x<0.2$), complex oxides and Zr-rich solid solution $(Zr_{1-x},Ce_x)O_2$ in the CeO_2–ZrO_2 system. Lattice constant of $(Ce_{1-x},La_x)O_{2-x/2}$ increased as La content, whereas that of $(Ce_{1-x},Zr_x)O_2$ decreased as Zr content. The result is explained by different cation radii of Ce^{4+}, La^{3+} and Zr^{4+} in oxide solid solution with the same fluorite-type structure.

CO oxidation activity of $(Ce_{0.9},La_{0.1})O_{1.95}$ and $(Ce_{0.8},Zr_{0.2})O_2$ heated at 1,000°C are shown in Fig. 8. The activity of CeO_2 is extremely improved by the addition of La and Zr into CeO_2. The reaction kinetics is controlled by the diffusion of lattice oxygen and is described by the following equation:

$$kt = \{1 - (1 - \alpha)^{1/3}\}^2 \tag{3}$$

where α is non-stoichiometric parameter in $CeO_{2-\alpha}$ and $(Ce_{0.8},La_{0.2})O_{1.9-\alpha}$ obtained by *in situ* XRD data (Ozawa *et al.*, 1991). This suggests that La addition enhances the activity of lattice oxygen for CO oxidation. Meanwhile, the particle diameter of $Ce_{0.8}Zr_{0.2}O_2$ heated at 1,000°C is 12 nm, which is much smaller than 1,100 nm of CeO_2. It is concluded that Zr addition prevents the sintering of CeO_2 and enhances the diffusion of lattice oxygen.

C. HEAT RESISTANT OXYGEN STORAGE MATERIAL: ACZ

A new material, that we named ACZ was developed for a TWC with high activity based on a novel concept, i.e. the diffusion barrier concept as described in Fig. 9 (Kanazawa *et al.*, 2003). Diffusion barrier layers of Al_2O_3 are built up between CeO_2–ZrO_2 mixed oxide (CZ) particles to inhibit the coagulation or grain growth of CZ. After an aging test at 1,000°C for 10 h in air, the surface area of ACZ was 29 m^2/g compared with that of CZ: 2 m^2/g. Table II shows the precious metal particle diameter and the crystal diameter of CZ in two catalysts.

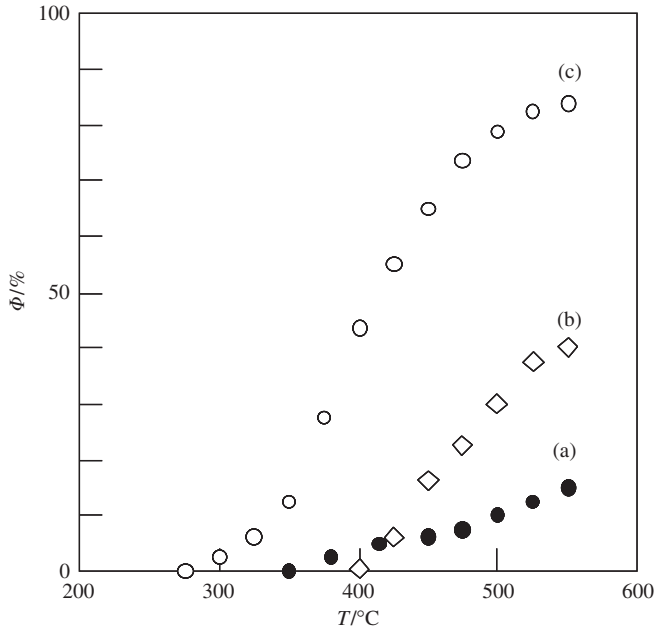

FIG. 8. Conversion (φ) of CO pulsed onto (a) CeO_2, (b) $Ce_{0.9}La_{0.1}O_{1.95}$ and (c) $Ce_{0.8}Zr_{0.2}O_2$ heated at 1,000°C for 5 h in air.

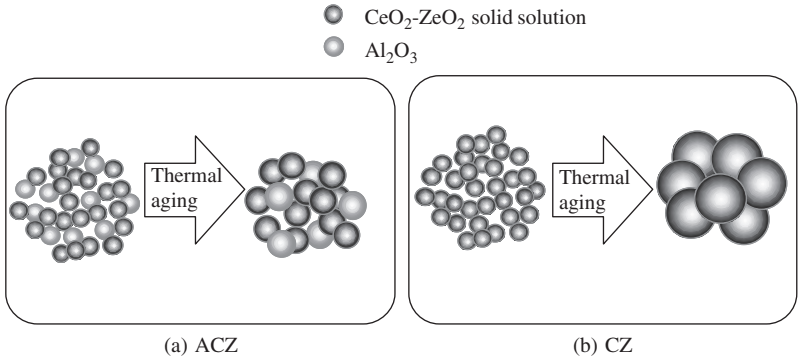

FIG. 9. The diffusion barrier concept for ACZ compared with CZ. (a) ACZ: the sintering of CZ is inhibited by Al_2O_3 particles dispersed among CZ particles and (b) CZ: sinter easily without any dispersal.

TABLE II
THE PRECIOUS METAL PARTICLE DIAMETER AND THE CRYSTAL DIAMETER OF CZ IN TWO CATALYSTS: CATALYST A CONTAINED 1.5 g/dm^3 Pt, 0.35 g/dm^3 Rh WITH CZ AND CATALYST B CONTAINED THE SAME AMOUNT OF PRECIOUS METALS WITH ACZ

Sample[a]	Particle (diameter/nm)[b]	
	CZ	Pt
A	17.2	23.7
B	8.7	19.6

[a]Aged at 950°C for 100 h.
[b]Measured by XRD.

TABLE III
LIGHT-OFF TEMPERATURE OF AGED CATALYSTS: CATALYST A CONTAINED 1.5 g/dm^3 Pt, 0.35 g/dm^3 Rh WITH CZ AND CATALYST B CONTAINED THE SAME AMOUNT OF PRECIOUS METALS WITH ACZ

Sample[a]	Light-off temperature[b] (°C)		
	HC	CO	NO_x
A	332	322	319
B	318	307	302

[a]Aged at 950°C for 100 h.
[b]Temperature at 50% conversion.

These catalysts were aged under the exhaust gas stream at 900°C for 100 h. Catalyst A contained 1.5 g/dm^3 Pt, 0.35 g/dm^3 Rh with CZ and Catalyst B contained the same amount of precious metals with ACZ. As shown in the table, both the sintering of the precious metals and the CZ particles is inhibited in Catalyst B compared with Catalyst A. Table III also shows the light-off temperature of those catalysts. The light-off temperature of Catalyst B is about 15°C lower than that of Catalyst A. In addition, the NO_x emission of a vehicle equipped with Catalyst B was about 20% less than that with Catalyst A.

D. ATOMIC ARRANGEMENT OF OXYGEN STORAGE MATERIALS AND THEIR OSC

Three types of CZ were prepared by Suda *et al.* to investigate the relations between the structures of these materials and their OSC properties (Suda *et al.*, 2001, 2002). M–CZ was prepared by the hydrolysis of an aqueous solution of $ZrO(NO_3)_2$ with ammonia on CeO_2 powder, followed by the calcination in air at 700°C. The structure of M–CZ was a mixture of CeO_2, ZrO_2 and CeO_2–ZrO_2 solid solution. S–CZ was prepared by an attrition-milling process of CeO_2

TABLE IV
COORDINATING CATIONS FOR Ce AND Zr OF THE CZ MATERIALS MEASURED BY XAFS ANALYSIS

	Sample		
A–B[a]	M–CZ	S–CZ	R–CZ
Ce–Ce	11.9	8.0	6.0
Ce–Zr	0.0	3.6	6.0
Zr–Ce	0.0	4.0	6.0
Zr–Zr	12.0	3.0	6.0

[a]A(center cation)–B(coordinating cation).

powder with ZrO_2 spheres in ethanol. The structure of S–CZ was a solid solution of CeO_2 and ZrO_2. R–CZ was prepared by the calcination of M–CZ with graphite at 1,200°C under a reducing atmosphere followed by the re-oxidation in air at 500°C. The structure of R–CZ was a solid solution of CeO_2 and ZrO_2 when the mole fraction of ZrO_2 was below 0.3. The κ-phase structure of $CeZrO_4$ was appeared when the mole fraction of ZrO_2 was above 0.3.

The arrangement of atoms in the local structure of CZ with 50 mole% of ZrO_2 was studied by Nagai *et al.* (2001, 2002). The number of nearest neighbor cations around Ce^{4+} or Zr^{4+} is shown in Table IV, which were determined from the data of Ce and Zr K-edge EXAFS. Both a Ce and a Zr atoms in R–CZ are surrounded by six Ce and six Zr atoms, respectively, via Ce–O–Ce, Zr–O–Zr or Ce–O–Zr bonds. The crystal structure of R–CZ was determined by XRD to be a pyrochlore-type structure, that is, Ce and Zr atoms were arranged regularly. On the contrary, the local structure around Ce is different from that around Zr in S–CZ and in M–CZ. Based on these experimental results, the schematic atomic arrangement of each CZ is shown in Fig. 10.

The amount of OSC for these oxygen storage materials described earlier was measured according to the following procedure. Platinum-loaded catalysts were prepared by impregnating M–CZ, S–CZ and R–CZ with a solution of $Pt(NH_3)_2(NO_2)_2$ into M–CZ, S–CZ and R—CZ, respectively. Pt of 1% was loaded onto each CZ material. These catalysts were treated at 900°C in air for 15 min, followed by reduction under a stream of 20% hydrogen in nitrogen at 500°C until the decrease of their mass ceased. Subsequently, they were re-oxidized under a stream of 50% oxygen in nitrogen until the increase of their mass ceased. The amount of mass decrease was almost equal to the increase for each catalyst, thus we defined this quantity as OSC of these materials. Figure 11 shows the specific OSC of the CZs, i.e. the amount of OCS per mole of Ce. The specific OSC of R–CZ has the maximum value of 0.22 mol(O_2)/mol(Ce), close to the theoretical value of 0.25, at 50 mole% of ZrO_2. The regular arrangement of Ce and Zr atoms in R–CZ with 50 mole% of ZrO_2 probably eases the oxygen release from it. In the oxygen-release process, the volume of the CZs increases in proportion to the change in the ratio of Ce^{4+} (smaller cation: 0.094 nm) to

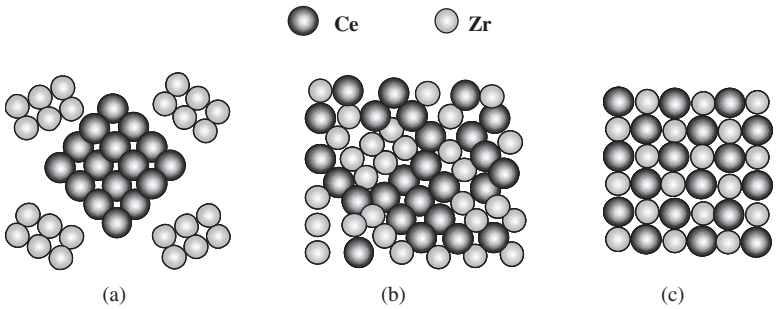

FIG. 10. Schematic figure of the atomic configuration of three types of CeO_2–ZrO_2 mixed oxide (CZ). (a) M-CZ was a mixture of CeO_2, ZrO_2 and CeO_2–ZrO_2 solid solution; (b) S–CZ was a solid solution of CeO_2 and ZrO_2 and (c) R–CZ was a solid solution of CeO_2 and ZrO_2 with a pyrochlore-type structure, that is, Ce and Zr atoms were arranged regularly.

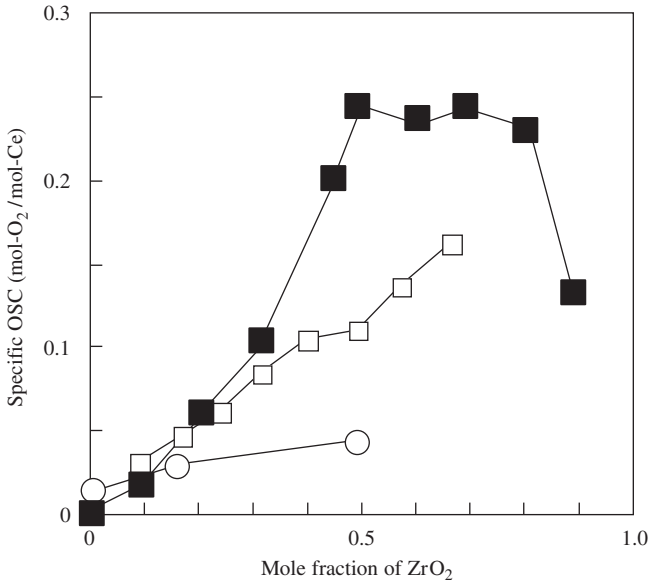

FIG. 11. Specific OSC of CeO_2–ZrO_2 mixed oxide (CZ) as a function of ZrO_2 content. ○, M–CZ; □, S–CZ; ■, R–CZ.

Ce^{3+} (larger cation: 0.114 nm). The stress energy caused by this volume change would suppress further valence change of Ce. The substitution of the smaller ion Zr^{4+} (0.084 nm) for Ce^{4+} could compensate for the volume change, which then could ease the valence change of Ce. The 8 in 64 oxygen atoms in the unit

cell of pyrochlore-type R–CZ crystal are surrounded by 4 Zr atoms. The other oxygen atoms are surrounded by both Ce and Zr atoms or by four Ce atoms. The 8 oxygen atoms would be easier to move than the other 56 atoms because they are completely surrounded by all of smaller Zr ions. The ratio of the mobile 8 oxygen atoms (4 oxygen molecules) to 16 Ce atoms in the unit cell of R–CZ with 50 mole% of ZrO_2 is consistent with the theoretical value of 0.25 mol(O_2)/mol(Ce) for the amount of OSC.

E. Dynamic Oxygen Mobility in Pt/CeO_2–ZrO_2

The oxygen mobility on three types of CeO_2–ZrO_2 mixed oxide (M–CZ, S–CZ and R–CZ) was studied by the $^{18}O/^{16}O$ isotopic exchange reaction combined with CO oxidation reaction (Dong *et al.*, 2004a, b).

1. Isotopic Exchange Reaction

Pt of 1 wt% was supported by conventional impregnation on M–CZ, S–CZ and R–CZ, respectively. The catalyst sample was reduced under hydrogen for 15 min at 500°C followed by the oxidation for 60 min at 500°C. The sample was cooled down to room temperature. A 50 Torr dose of pure $^{18}O_2$ was then introduced at the reaction temperature. The pressure of the oxygen isomers, P-36 ($^{18}O_2$), P-34 ($^{18}O^{16}O$) and P-36 ($^{16}O_2$) was continuously measured at the temperature of reaction.

The partial pressure curves of three molecules evolved from Pt/R–CZ along with the exchange reaction at 460°C are plotted in Fig. 12 (Dong *et al.*, 2004a). At 460°C, the adsorption and decomposition of oxygen molecules on Pt would be very fast, thus the diffusion of oxygen atoms to the top surface from the bulk oxide would be the control step. The initial reaction region is referred to as Zone 1 corresponded with the surface diffusion, and the reaction region approaching equilibrium is referred to as Zone 2 ascribed to the bulk diffusion.

Isotopic exchange reaction rates and oxygen diffusion coefficients of Pt/M–CZ, S–CZ and R–CZ at 411°C are listed in Table V (Dong *et al.*, 2004a). The surface diffusion rate for R–CZ (R_E^0) is nearly 4 times larger than the bulk diffusion rate or the equilibrium isotopic exchange rate (R_E^∞), while it is 3.8 times larger for S–CZ and 26 times larger for M–CZ. These results indicate that the contribution from bulk could also be counted as an important function in the total oxygen and release performance. As listed in Table V, the derived surface and bulk oxygen diffusion coefficients of R–CZ are apparently larger than those of S–CZ and M–CZ. This indicates that the surface and bulk diffusion coefficients relate closely with the nature and structure of the oxygen storage material.

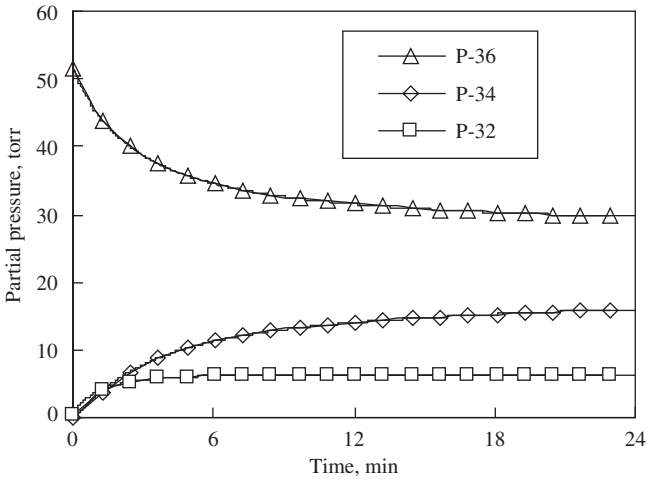

FIG. 12. Partial pressure evolution during isotopic exchange reaction on CZ–R at 460°C.

TABLE V
ION EXCHANGE REACTION AND OXYGEN DIFFUSION COEFFICIENTS AT 411°C

Catalysts	Pt/R–CZ	Pt/S–CZ	Pt/M–CZ
Initial ion exchange reaction rate, R_E^0, (atoms/s/g)	1.504×10^{18}	3.899×10^{17}	1.578×10^{18}
Equilibrium ion exchange reaction rate, R_E^∞, (atoms/s/g)	3.55×10^{17}	1.029×10^{17}	5.7321×10^{16}
Surface diffusion coefficient, D_S (m^2/s)	2.98×10^{-13}	1.48×10^{-18}	4.23×10^{-19}
Bulk diffusion coefficient, D_B (m^2/s)	4.33×10^{-19}	1.20×10^{-20}	7.77×10^{-22}

2. *Dynamic Oxygen Storage and Release Performance and the Role of Zr*

Following the $^{18}O_2/^{16}O_2$ isotopic exchange reaction of the catalyst sample, CO was introduced into the system to conduct CO oxidation reaction as shown in Fig. 13. From the sum of the production of $C^{16}O_2$ and $C^{16}O^{18}O$ and their production rate in Fig. 13, the oxygen storage capacity and the oxygen release rates are derived as shown in Fig. 14 (Dong *et al.*, 2004b). The obtained oxygen storage capacity and oxygen release rate are well matched with the results measured by thermogravimetric analysis (TGA) method (Suda *et al.*, 2000, 2001), and are in good agreement with the oxygen mobility obtained from the isotopic exchange reaction. Moreover, these parameters are consistent with the structural homogeneity of Zr in the framework of the oxides, as R–CZ > S–CZ > M–CZ.

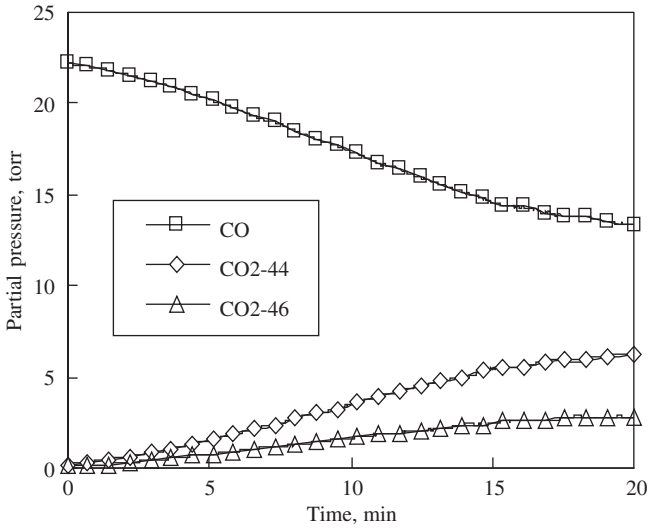

FIG. 13. Subsequent CO oxidization at 500°C after isotopic exchange reaction on R–CZ at 460°C.

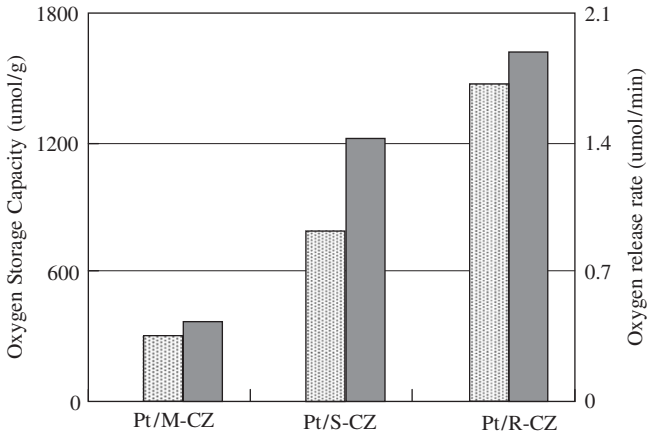

FIG. 14. Oxygen storage capacity and oxygen release rates at 500°C.

Based on the isotopic exchange reaction, the oxygen diffusion coefficients of the pure CeO_2, $Ce_{0.15}Zr_{0.85}O_2$ oxide and the pure ZrO_2 were measured as in Table VI (Dong *et al.*, 2004a). The table clearly indicates that the surface diffusion coefficient of CeO_2 is much higher than that of ZrO_2, while the bulk diffusion coefficient is smaller than that of ZrO_2. The CeO_2–ZrO_2 solid solution

TABLE VI
OXYGEN DIFFUSION COEFFICIENT IN CeO_2–ZrO_2 OXIDES

Oxides	CeO_2	$Ce_{0.15}Zr_{0.85}O_2$	ZrO_2
D_S at 300°C (10^{-19} m^2/s)	21	33	2
E_a (kJ/mol)	41	39	49
D_B at 300°C (10^{-23} m^2/s)	12	53	41
E_a (kJ/mol)	15	10	14

gives both a much higher surface and bulk diffusion coefficient. These results suggest that zirconium atoms in the framework not only contribute to the enlargement of the lattice space for the migration of oxygen atoms as described in the last section but also help to capture oxygen atoms and transfer them to cerium atoms.

IV. Sintering of PGM

A. Introduction

Platinum group metals (PGM) such as Pt, Pd and Rh have been used in conventional TWCs. The catalytic performance of TWCs deteriorates accompanied with sintering of PGM caused by thermal aging during car driving. The effect of aging temperature and atmosphere on the catalytic activity and the sintering of Pt, Pd and Rh on alumina support were investigated under the synthesized gas stream (Shinjoh *et al.*, 1990). For Pt and Rh, the catalytic activity decreases and the particle size increases with increasing both aging temperature and the oxygen concentration in the aging atmosphere. However, for Pd, the effect of the oxygen content on the catalytic activity and the sintering is the reverse as compared with that of Pt and Rh. The characterization of Pt/Rh TWCs aged under the engine exhaust stream and the improvement of their heat resistance were reported by Miyoshi *et al.*, 1989. The particle size of PGM increases with increasing aging temperature and aging time. The surface area of alumina support and the catalytic performance decreases simultaneously. The addition of about 1 mole% of La into alumina suppresses the loss of its surface area, and then the sintering of Pt and Rh is highly restricted.

The performance of TWC and its durability should be further improved to meet the new requirements for low-emission vehicles. It is described in this chapter that the sintering of Pt depends on the characteristic of supports and the re-dispersion of Pt is occurred on CeO_2 through the interaction between Pt and the surface oxygen of CeO_2.

B. Sintering Inhibition Mechanism of Platinum Supported on Ceria-based Oxide

The sintering of Pt after high-temperature aging in an oxidative atmosphere is much higher than in a reductive atmosphere (Fiedorow *et al.*, 1978; Harris, 1986). The sintering of Pt particles on various oxides in an oxidative atmosphere was investigated at the atomic level using X-ray absorption analysis (Nagai *et al.*, 2006).

Figure 15 shows the transmission electron microscopy (TEM) images of the Pt/Al_2O_3 and Pt/CZY catalysts after aging treatment at 800°C in air for 5 h. In the aged Pt/Al_2O_3, large Pt particles ranging from 3 to 150 nm are observed. In contrast, no explicit Pt particles are observed on the aged Pt/CZY. In the aged Pt/CZY, Pt was detected by energy dispersive X-ray (EDX) analysis. This indicates that Pt particles are highly dispersed on the CZY support. The average size of Pt metal particles for these catalysts determined by XRD and the CO pulse method is shown in Table VII. Pt particle size on the Al_2O_3 support before the aging treatment, as estimated by the CO pulse method, is almost the same as that on CZY (about 1 nm diameter). Pt particle size increased significantly in Pt/Al_2O_3 during the aging treatment; particle sizes in the aged Pt/Al_2O_3 determined by XRD and CO pulse methods are 61 and 23.6 nm, respectively. However, Pt particles in the Pt/CZY cannot be observed by XRD even after aging, suggesting that the Pt particles on CZY support remain highly dispersed. The Pt particle size of 1.1 nm in the aged Pt/CZY estimated by CO pulse is the same as that in the fresh catalyst.

The local structure around a target element is revealed by EXAFS analysis. The Fourier transforms (FTs) of the aged catalysts and reference samples

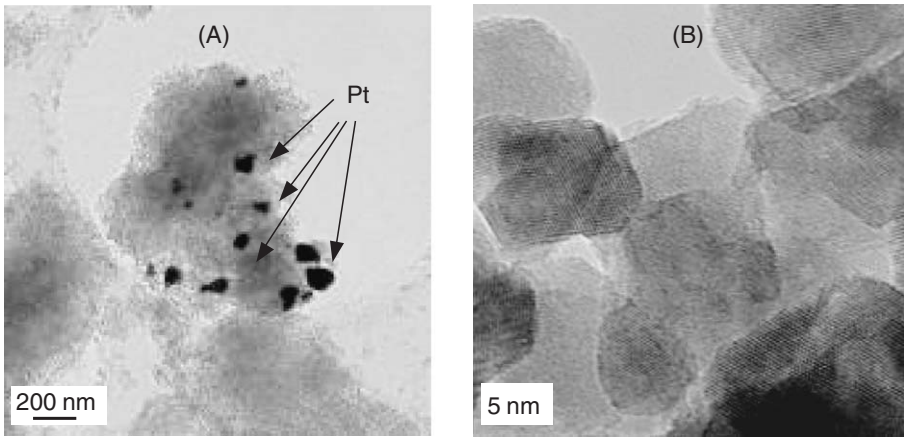

Fig. 15. TEM images of Pt supported catalysts after 800°C aging in air for 5 h. (A) Pt/Al_2O_3 catalyst and (B) Pt/CZY.

TABLE VII
AVERAGE PLATINUM PARTICLE SIZES OF THE CATALYSTS ESTIMATED BY XRD AND CO ADSORPTION

Sample	Average Pt particle size (nm)	
	XRD[a]	CO adsorption
Pt/Al_2O_3		
Fresh	ND[b]	1
Aged	61	23.6
Pt/CZY		
Fresh	ND[b]	1.1
Aged	ND[b]	1.1

[a]Average particle size was estimated from Pt(111) line width.
[b]The diffraction peak from the Pt particles could not be detected.

performed on the Pt L3-edge EXAFS spectra in the ca. 3.0–16 $Å^{-1}$ region are presented in Fig. 16. The quantitative curve-fitting analysis of the EXAFS spectra was performed for the inverse FTs on the Pt–oxygen and Pt–cation (cation = Pt, Ce and Zr) shells, respectively. In the FT spectrum of Pt foil, the peak at 2.76 Å is assigned to the Pt–Pt bond. FT spectrum of PtO_2 powder, the peaks at 2.04 and 3.10 Å are assigned to the Pt–O and Pt–O–Pt bonds, respectively.

For an aged Pt/Al_2O_3 sample, only an intense peak at 2.76 Å, which corresponds to the Pt–Pt bond, was observed. The FT spectrum of the Pt/Al_2O_3 coincides with that of Pt foil. The coordination number (CN) of the Pt–Pt shell in the aged Pt/Al_2O_3 sample was 11.5. This indicates that the Pt metal particles on Al_2O_3 after aging are at least 20 nm in size (Greegor and Lytle, 1980). For Pt supported on CZY (solid solution of 50 wt% CeO_2, 46 wt% ZrO_2 and 4 wt% Y_2O_3) analyzed after the aging treatment, two peaks are observed. The first peak at 2.02 Å is assigned to the Pt–O–Ce bond, and the second peak at 1.7 Å is assigned to the Pt–O bond by comparison to a PtO_2 reference. The value of the CN of the Pt–Ce shell in aged Pt/CZY was 3.5. This coordination number of 3.5 is lower than 12, which is the maximum coordination number in the cubic fluorite structure. This indicates that Pt ions exist on the surface of the CZY support. In addition, intense Pt–Pt or Pt–O–Pt peaks could not be observed in the aged Pt/CZY sample, suggesting that there are no large Pt metal or oxide particles on the CZY surface. In other words, highly dispersed Pt oxides are present on the surface of CZY.

Based on the observation earlier, the sintering inhibition mechanism of Pt supported on CZY is proposed as follows (Nagai *et al.*, 2006). In the case of Pt/Al_2O_3, since the interaction between Pt and Al_2O_3 is weak, mobile Pt particles migrate across the surface of the Al_2O_3 support and sinter during an 800°C aging treatment in an oxidizing atmosphere. In contrast, Pt supported on CZY has a strong interaction with the CZY support. Therefore the CZY support stabilizes a high-oxidation state of Pt, and then the formation of the

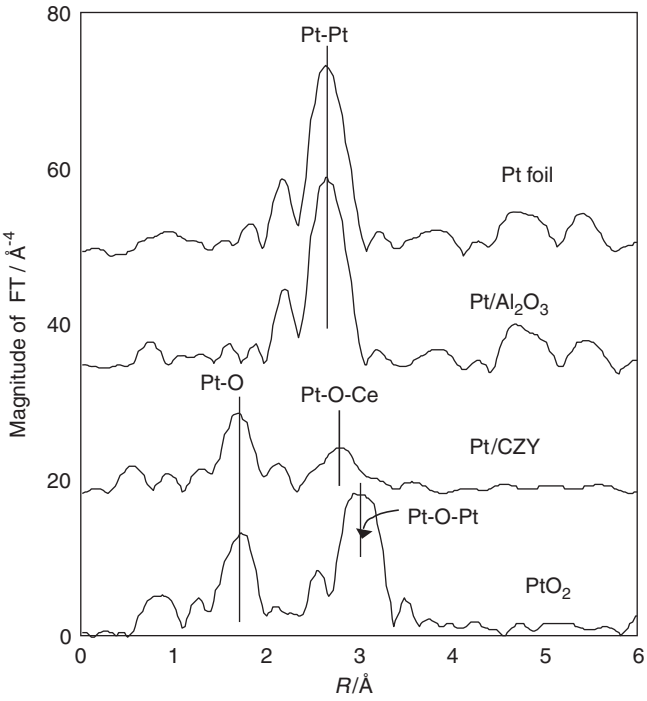

FIG. 16. Fourier-transformed k3x data of Pt L3-edge EXAFS for supported Pt catalysts after 800°C aging in air and the standard samples of Pt foil and PtO_2 powder.

rigid Pt–O–Ce bond acts as an anchor. The formation of the Pt–O–Ce bond on the CZY suppresses the sintering of Pt.

The average size of the Pt metal particles after the aging treatment under the oxidizing atmosphere on SiO_2, Al_2O_3, ZrO_2, TiO_2, CeO_2 and CZY was estimated using the CO pulse method. Also, the binding energy of the O(1s) electron in those support oxides was measured by XPS analysis. The XANES spectra of the L3-edge of Pt on these oxides were investigated. There is a linear relationship between the white-line intensity in the XANES spectra and the oxidation state of PtO_x on some metal oxide supports (Yoshida *et al.*, 2005). On the basis of this linear relationship, the oxidation state of Pt on Al_2O_3 was estimated as 0, and as 3.53 on CZY, etc. Figure 17 shows the correlation between these three factors on the various supported Pt catalysts. It is clear that there is a very strong correlation between these three factors. The oxidation state of Pt after aging increased with the decreasing binding energy of the O(1s) electron. This indicates that the Pt-oxide-support interaction strengthens as the electron density of oxygen in support oxide increases, that is, Pt particles on the electron dense support oxide are oxidized easily. Subsequently, the Pt

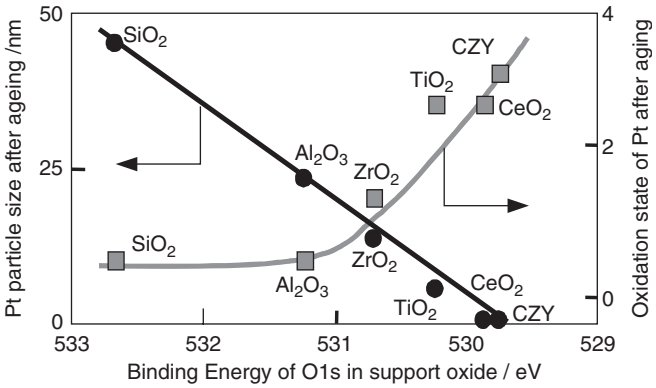

FIG. 17. Pt-oxide-support interaction and its relation to Pt sintering in an oxidizing atmosphere.

particle size after the aging decreases as the electron density of oxygen in the support increased. As a result, the sintering inhibition effect on Pt can be controlled by the electron density of oxygen in the support oxide through the Pt-oxide-support interaction. That is the key parameter of the Pt-oxide-support interaction and its relation to Pt sintering in an oxidizing atmosphere.

C. Re-dispersion of Platinum Supported on Ceria-based Oxide

Nishihata *et al.* (2002) reported the re-dispersion of Pd in a Perovskite-type oxide. They investigated the oxidation state and the local structure of Pd by using X-ray absorption analysis. Pd occupies the B-site in La_2PdCoO_6 in the oxidized sample. For the reduced catalyst, the XAD and XANES measurements suggested the segregation of metallic Pd from the perovskite crystal. They imply that Pd also moves back and forth between the B-site in the perovskite structure and sites within the lattice of Pd metal clusters dispersed on perovskite surface when the catalyst is exposed to fluctuations in the redox characteristics of the emission exhaust.

The re-dispersion phenomena of sintered Pt on CZY were observed by *in situ* time-resolved Turbo-XAS in fluorescence mode at ID-24 of ESRF (Nagai *et al.*, 2006). H_2 (3%) (He balance) and O_2 (20%) (He balance) gases were introduced to the *in situ* sample cell alternately every 60 s. The white-line peak height of the normalized Pt L3-edge XANES for the sintered Pt/CZY catalyst was collected every 1 s, which is plotted in Fig. 18. The white-line peak height changes very quickly, within 1 s, between the values of reduced and that of oxidized Pt after switching the gas atmosphere. This result indicates that the reduction and oxidation of Pt is very fast. While the white-line peak height under the reducing atmosphere is constant, the height under the oxidizing atmosphere increases

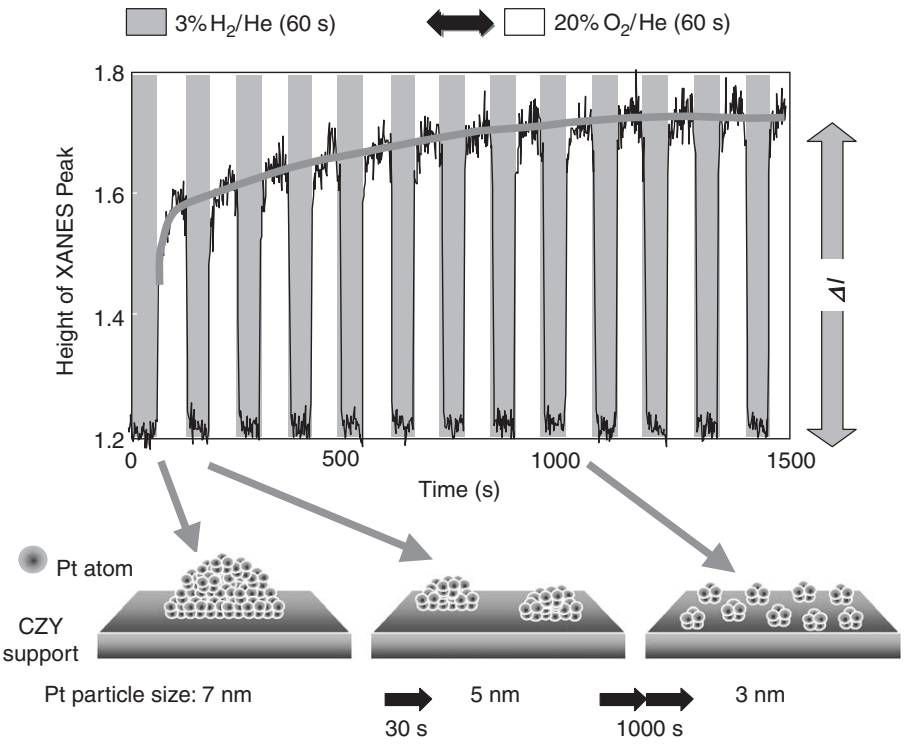

FIG. 18. Time resolved height of the XANES peak for the sintered Pt/CZY catalyst (Pt particle size; 7 nm) under oxidizing/reducing atmosphere at 600°C.

gradually. The difference between the white-line peak height of the oxidized and reduced samples corresponds with the particle size of Pt as shown in Fig. 19 (Nagai *et al.*, 2006). Therefore, it is indicated that the Pt particle size of the aged catalyst decreases from 7 to 5 nm after 60 s, and then to 3 nm after 1,000 s. This kind of Pt re-dispersion was not observed in a conventional Pt/Al_2O_3 catalyst. These results suggest that the Pt particle on CZY is easily oxidized under the 20% O_2 gas stream through the strong Pt-ceria-support interaction followed by breaking into small pieces of oxide particles, i.e. Pt re-dispersion.

V. NO_x Storage and Reduction Catalyst and Reaction Mechanism

A. NO_x Reduction Method Under Lean Conditions

Along with the concern in the pollutants of NO_x, CO and HC, the care about the emission of CO_2 is also increasing. Today, fuel-efficient lean-burn engines

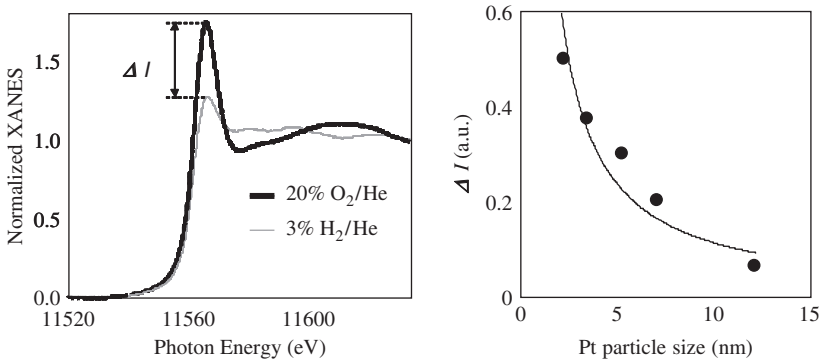

FIG. 19. Pt L3-edge XANES of a Pt/CZY catalyst under oxidizing/reducing atmosphere at 400°C (left). Relationship between Pt particle size and ΔI (right).

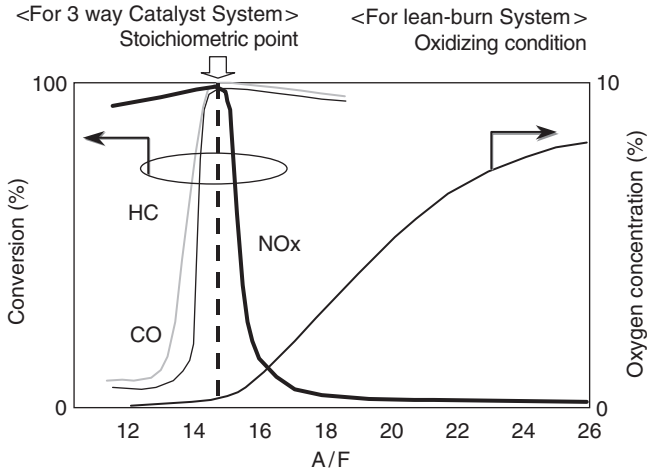

FIG. 20. Performance of a conventional 3-way catalyst.

have been widely adopted. Figure 20 shows the performance of a conventional TWC. Under oxidizing conditions in the lean-burn exhaust gas, the TWC acts as an oxidation catalyst efficiently controlling CO and HC emissions, but the conversion of the NO_x emissions falls to very low levels.

The NO_x reduction for the exhaust from lean-burn engine is one of the greatest challenges in environmental protection, and a lot of researchers have strived to develop more effective catalysts by many ways. Their efforts could be possibly categorized into four approaches: (1) NO_x direct decomposition, (2) selective catalytic reduction on NO_x with hydrocarbons (HC–SCR), (3) selective catalytic reduction on NO_x with ammonia (NH_3–SCR) and (4) NO_x storage and reduction (NSR).

(1) NO_x direct decomposition seems the most attractive solution in emission control, because the reaction does not require any reductants added and potentially could lead to the formation of only N_2 and O_2. Cu–zeolite is one of the best catalysts for NO_x direct decomposition, but the activity is very poor and needed to be improved several orders of magnitude high (Iwamoto *et al.*, 1981).
(2) HC–SCR is a desirable way for the use of very similar type of hydrocarbons that could be found in exhaust gases, and lots of papers have been published (Burch and Watling, 1996; Hamada *et al.*, 1990; Held and Konig, 1990; Iwamoto *et al.*, 1990). Many types of catalyst, in particular Cu–zeolites, alumina, Pt-loaded catalysts, show HC–SCR activities and have an operation window for NO_x reduction as a function of temperature, respectively. That is because NO_x reduction with HC is competitive to HC oxidation with O_2 in the oxidizing conditions. Catalyst for automotive exhaust is subjected to have high activity through a wide operating condition, therefore, HC–SCR catalyst has not yet used practically for automotive pollution.
(3) NH_3–SCR is a mature technology for steady-state conditions from power plant and stationary diesel engines (Forzatti, 2001), while is not sufficient for mobile applications, in particular motor vehicles, the catalyst is operated under fast transient conditions, and exposed to exhausts of a large temperature range. Though V–W/Ti, Cu(or Fe)–zeolite catalysts are candidates for NH_3–SCR, some problems are sticking out, such as the facility for carrying urea as NH_3 source on board, and the social facility for urea supply (Johnson, 2001).
(4) NSR is very attractive method for NO_x removal by storing NO_x under lean conditions and then reducing the stored NO_x to N_2 under rich excursions by engine operation: this technology is also referred as a lean NO_x trap. In this chapter, NSR catalyst and the mechanism for NO_x reduction is described.

B. Outlook of NSR Catalyst

The NSR catalysts are mainly composed of precious metals as active site, basic materials such as barium compounds for NO_x storage, and large surface oxides as support. Figure 21 illustrates the reaction mechanism of NO_x storage and reduction on the catalyst. Under oxidizing conditions, NO is first oxidized on precious metals and stored as nitrates on the neighboring NO_x storage compounds. Subsequently, the stored NO_x is reduced to nitrogen by the following two steps: decomposition of nitrates and then reaction with reducing agents on the precious metals. Figure 22 (a) illustrates the schematic diagram of lean-burn gasoline system commercialized in Japan, and Fig. 22 (b) shows an

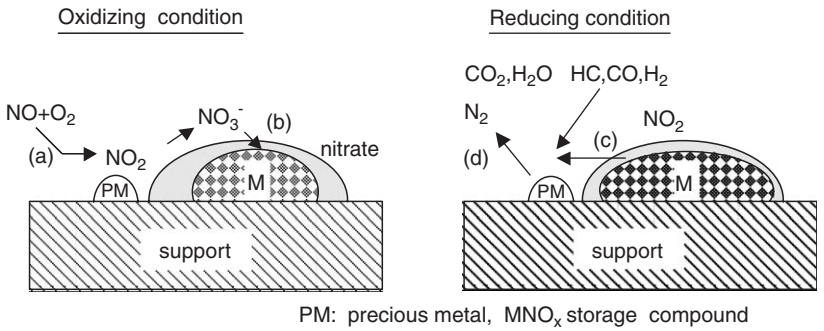

FIG. 21. NO_x storage and reduction scheme on NSR catalyst.

example of air and fuel mixture control methods during constant cruising (Kato *et al.*, 1994). As the figure shows, NO_x concentration in the outlet gas becomes higher with time in lean-burn condition at A/F = 23, which means the catalyst becomes to be saturated with NO_x. A rich mixture supply at A/F = 10 at a certain interval reduces the stored NO_x effectively with very little fuel penalty.

C. MECHANISM OF NSR CATALYST

Recently, the mechanism of NO_x adsorption and desorption, reduction on NSR catalyst has been investigated by a lot of scientists (Epling *et al.*, 2004; Fridell *et al.*, 1999, 2000; Lietti *et al.*, 2001; Takahashi *et al.*, 1996, 2006). It appears now clearly the storage/reduction is rather complex process due to the complex nature of the exhaust gases. However, four reactions described later are believed to be the main routes with the NSR reaction: (a) NO oxidation to NO_2 (oxidizing condition), (b) NO_x storage on basic material (oxidizing condition), (c) NO_x release from the basic material (reducing condition) and (d) NO_x reduction to N_2 (reducing condition).

(a) This route proceeds on oxidation catalysts at low temperature being restricted due to the thermodynamic equilibrium of NO and NO_2. It is well known that Pt catalysts promote NO oxidation significantly in oxidizing condition, while its behavior in lean-burn exhaust is a little bit different (Piacentini *et al.*, 2005). The residual agents of CO and hydrocarbons in oxidizing condition reduces NO_2 to NO on the catalyst; hence, the outlet NO_2 concentration falls lower than the value merely derived from thermodynamic equilibrium with NO oxidation reaction (Fig. 23). With CO or hydrocarbons existing in the reaction atmosphere, it does not matter

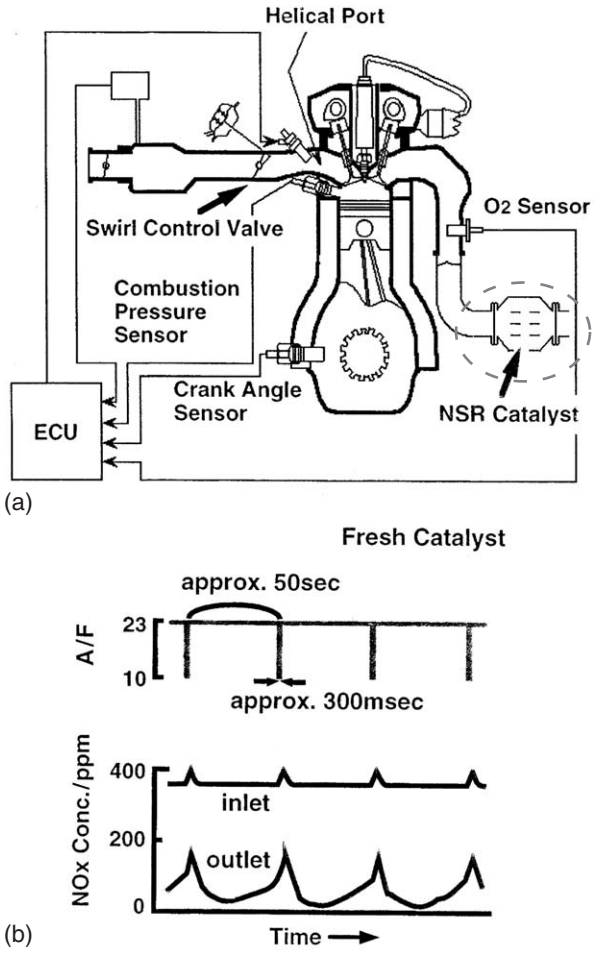

FIG. 22. (a) Schematic diagram of lean-burn gasoline system with NSR catalyst. (b) Rich mixture control method during constant speed driving.

if NO_2 or NO is used as the inlet NO_x species; the outlet NO_2 concentration would turn out the same. Thus, the NO_x storage amount with NO_2 as an inlet NO_x source is approximately the same as that with NO. If CO or hydrocarbons is not present in the reaction condition, the outlet NO_2 concentration equals to the thermodynamic value with NO oxidation reaction, resulting in the increase of NO_x storage amount on the catalyst. Therefore, both NO oxidation to NO_2 and the removal of the residual reducing agents from exhaust gas are necessary for improving the NO_x storage performance at low temperature.

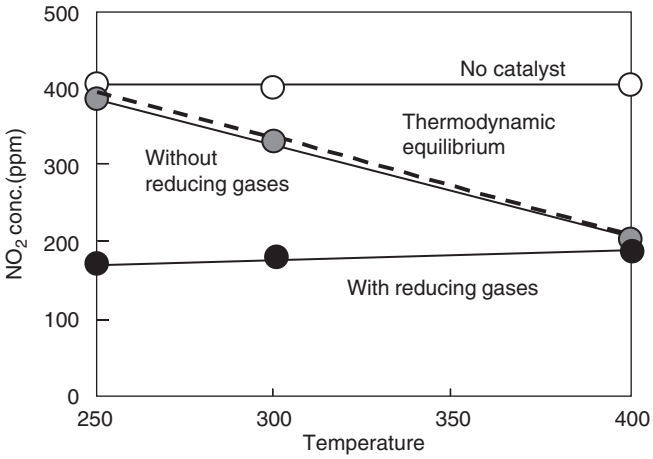

FIG. 23. Effect of H_2 and CO coexistence for NO_2 formation on the NSR catalyst in oxidizing condition.

(b) Comparing the Fourier transform infrared (FTIR) spectra before and after NO_x storage on the Pt/Ba catalyst, the majority of NO_x stored is a nitrate species, in particular at high temperature due to the low thermal stability of nitrite (Takahashi *et al.*, 1996). The pathways for NO_x storage exist in both nitrite and nitrate routes (Epling *et al.*, 2004; Fridell *et al.*, 2000). The nitrite route implies a stepwise oxidation of NO on precious metal followed by adsorption at a neighboring Ba site to form a nitrite ad-species that is then oxidized to a nitrate. The nitrate pathway implies nitrates form through the disproportionation reaction of NO_2. The nitrite route seems to occur on Ba site near precious metal, so that is considered more effective and the main route under the actual exhaust conditions. The earlier consideration was derived from a simple reaction gas system, for example NO–O_2 reaction, although there exists much amount of CO_2 and H_2O in the exhaust gases. The kinetics and amount of NO_x storage are highly affected by the presence of CO_2 and H_2O (Epling *et al.*, 2004; Fridell *et al.*, 1999; Lietti *et al.*, 2001). It was shown that BaO, $Ba(OH)_2$ and $BaCO_3$ coexist at the surface on the Pt/Ba/Al_2O_3. NO_x storage occurs first at the Ba sites in the oxide form, then the hydroxide and finally the carbonate. CO_2 strongly competes with NO_x for the adsorption sites, thus decreases the NO_x storage amount on the catalyst. The effect of H_2O is reported to have both faces, promote or suppress depending on temperature. The promotion effect of H_2O was observed at low temperature, whereas at high temperature an inhibition effect was observed. There is a general agreement that the fraction of Ba involved in the NSR process is a small portion of the total loading in the catalyst, and the Ba loading amount affects the NSR behavior. Ba loading effect of Pt–Ba/Al_2O_3 catalysts was investigated with calcinations of the catalysts

(Piacentini *et al.*, 2005). It was resulted that there were three different Ba-containing species; amorphous BaO on Al_2O_3 surface, amorphous carbonates and crystalline carbonate. Amorphous carbonate showed relatively low thermal stability and possesses high reactivity for NO_x storage.

(c) NO_x release from the catalyst is caused by atmosphere change from oxidizing to reducing condition. There are two primary forces for NO_x release on the catalyst. One is generated by exothermic reactions such as oxidation of the reductant in the stream. NO_x can be released since the nitrate stability decreases with increasing temperature. The second cause is the introduction of the reductant species to achieve a net reducing environment. That is, the equilibrium stability of nitrate species is dramatically reduced. This route is also accelerated by Pt coexistence with promoting the reactions.

(d) The bottleneck step for the entire NSR process should be a reduction of the stored NO_x as low fuel penalty as possible, that means of a restricted rich condition. It is very important to clarify the reduction reaction in the NO_x reduction process. Figure 24 shows NO_x reduction abilities of reducing agents, H_2, CO and C_3H_6 (Takahashi *et al.*, in press). The order of the activities is the following: $H_2 > CO > C_3H_6$. And, the H_2 generation is more apparent and efficient by water gas shift reaction than that through the steam reforming reaction on the NSR catalyst. As described earlier, CO_2 competes with NO_x for adsorption on Ba site. This competition increases the rate of NO_x releases under reducing condition.

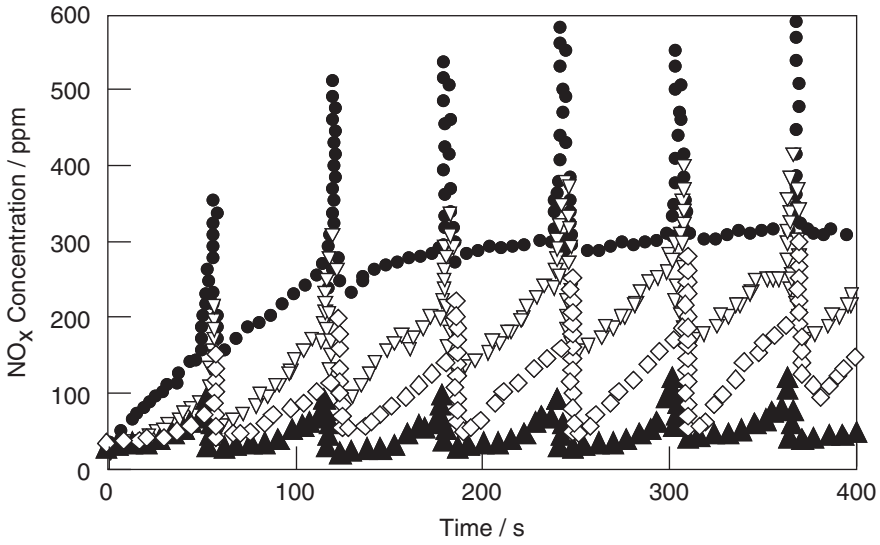

FIG. 24. Effect of reducing gas species for NSR reaction behavior at 250°C. Reducing gas: none (●), C_3H_6 (▽), CO (◇) and H_2 (▲).

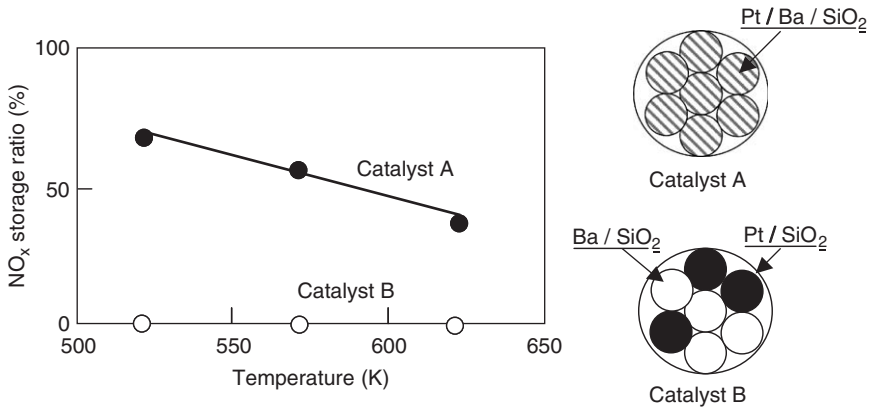

FIG. 25. Effect of arrangement with precious metal and NO_x storage compound to NO_x storage ratio.

Reaction (b) and (d) involves the spillover processes of NO_x between precious metal and NO_x storage site. The importance of close contact between Pt and Ba material was investigated through comparison of catalyst systems in which the two components are arranged differently (Fig. 25) (Takahashi *et al.*, 1996). Catalyst A was synthesized by supporting Pt and Ba on identical SiO_2 support particle. However, Catalyst B was prepared by blending Pt/SiO_2 and Ba/SiO_2. Figure 25 indicates the NO_x storage on the Catalyst A and B. This result suggested that Pt and Ba should be well contacted for high NO_x storage and the spillover process of NO_x between them is very important for NSR reaction. Under NO_x storage conditions, isotopic exchange between ^{15}NO and stored NO_x was investigated, and the exchange rate was much faster for a close Pt/BaO coexisting on the Al_2O_3 support than for a combined $Pt/SiO_2 + BaO/Al_2O_3$ system (Cant *et al.*, 2006). These results demonstrate that Pt and BaO in close proximity are essential for high spillover of NO_x between them. The distance between Pt and BaO available for NSR reaction was investigated using a simple model catalyst on a flat substrate and a thin film by several analysis methods; EPMA, SEM, TEM, EELS, XPS and AES. The stored NO_x was reduced in the region of a few micrometers around the Pt particle, after NO_x adsorption on the catalyst followed by the H_2 reduction for 1 h (Sakamoto *et al.*, 2006).

D. SO_x Poisoning

The NSR technology is regarded as the most reliable and attractive de-NO_x method. However, catalyst degradation by SO_x poisoning is a big problem. Sulfate was detected on the NSR catalyst after the aging test. SO_2 is oxidized and reacts with the NO_x storage materials to form sulfates, which means the

occupation of NO_x storage site. In general, sulfates are invariably more thermal stable compared to the nitrates, and a sulfated catalyst requires high temperature to be reduced, i.e. to be regenerated, that may induce a thermal degradation of the catalyst. The model catalyst of flat substrate with Pt and BaO as described earlier was used to investigate the difference between NO_x and SO_x adsorption–desorption behavior (Sakamoto *et al.*, 2006). Based on these experiments for the model catalyst, Fig. 26 shows that the NO_x adsorption–desorption site around Pt edge is about a few micrometers in the storage-reduction process of 1 h, however, the SO_x site is decreased for a few nanometers. This means that BaO within a few micrometers around the Pt can work as a NO_x storage material without SO_x poisoning. However, few nanometers of $BaSO_4$ close to Pt can be reduced, that is, only few nanometers of Ba layer around Pt edge can work as a storage material after SO_x poisoning. The length of diffusion of NO_x and reductants in a real vehicle driving condition, i.e. storage-reduction process in few seconds, should be much shorter than a few micrometers. Duprez (2006) reported that oxygen diffusion coefficient at 400°C on a series of Rh/oxide catalysts was in the range of 2×10^{-20}–$4 \times 10^{-16}\,m^2/s$. It means that oxygen atoms may migrate over distances around 10^{-10}–$10^{-8}\,m$ for 1 s. It will be a future challenge to quantify an effective site for the NSR process, however, the remarkable difference of adsorption–desorption behavior between NO_x and SO_x suggests that the NSR process should be blocked significantly after SO_x poisoning.

Figure 27 shows the relationship between the particle size of sulfate and their decomposition rate on an NSR catalyst (Takahashi *et al.*, 1996). The smaller the sulfate size is, the easier the decomposition. It was also reported that the sulfate size was strongly related to SO_x amount in the exhaust. As for reducing

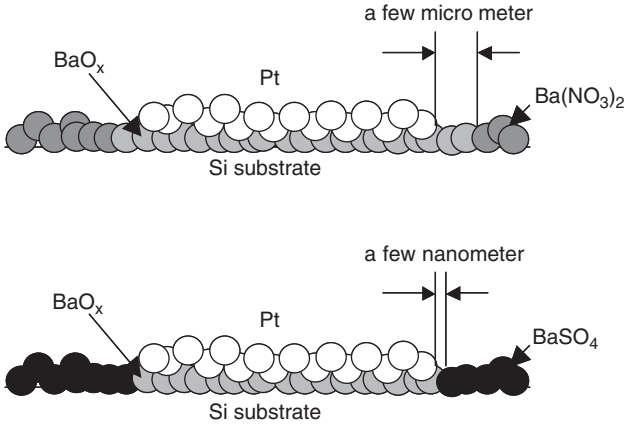

FIG. 26. Image of reduction area of nitrate and sulfate of barium around Pt.

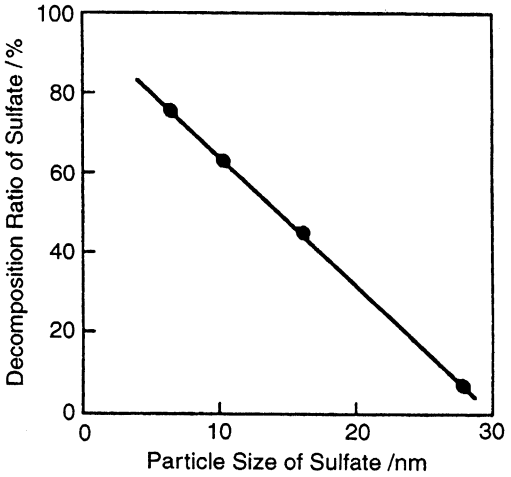

FIG. 27. The relationship between particle size and decomposition rate of barium sulfate on the NSR catalyst.

species, hydrogen has a much greater reducing power among reducing agents such as CO and HC (Matsumoto, 2004).

From these results, though it is not easy to decompose the sulfates, there are some directions to solve the problem. They are, (1) increase the number of active site by loading more and dispersing finely on the support, (2) improve the reducing condition which the NSR catalyst is exposed and (3) decrease the S content in fuel. However, increasing precious metal usage and reducing condition are not preferred from the point of view of environmental protection and effective use of valuables. So it is important to develop NSR catalysts with higher the SO_x durability, meanwhile, more efforts in oil industry are necessary to lower sulfur content in the fuel. In the next chapter, the progress on improving NSR catalysts and on NSR catalyst system will be described.

VI. Improvement of NSR Catalyst and Engine System

A. NSR Catalyst Formulation

An NSR catalyst consists of precious metal as active site, basic material as NO_x storage site, and support for highly dispersing these sites. As active site, Pt and Rh are much effective elements for NSR catalysts. One important role of the active site is to oxidize NO under oxidizing condition. Our early catalyst test showed that, precious metals and Mn oxide loaded on alumina are indicated a high NO oxidation activity. Particularly, Pt showed the highest turn over

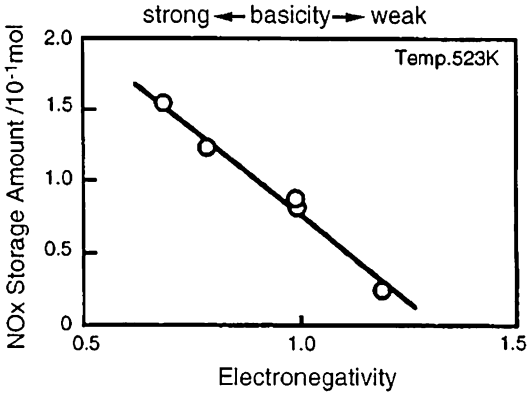

FIG. 28. The relationship between basicity of NO_x storage compounds and NO_x storage amount.

frequency compared with other elements. The other role of the active site is to reduce NO_x to N_2. Precious metals, in particular, Rh is well known as the best element for NO_x reduction activity. In addition, oxidation activities for HC and CO in exhaust gases are also necessary as automotive catalysts, Pt and Pd are suitable for oxidation. Therefore, NSR catalyst in general contains Pt and Rh, possibly Pd.

As NO_x storage material, basic materials as alkaline and alkaline earth compounds are popular in use. Figure 28 shows the influence of basicity of NO_x storage compounds on NO_x storage amount (Takahashi *et al.*, 1996). A close correlation between the NO_x storage amount and electron negativity is obtained, and stable nitrates can be formed with the strong basicity of NO_x storage compounds. Barium compounds have been used widely for high NO_x storage ability and its thermal stability. Potassium compounds are another component with a significant benefit at higher temperatures where the potassium nitrate is more stable than the typical barium nitrate (Konsolakis and Tentekakis, 2001; Toops *et al.*, 2006).

Support for NO oxidation reaction was reported that SiO_2 seemed to be preferable (Xue *et al.*, 1996). However, NSR catalysts are subjected high thermal stability like as the conventional automotive catalyst. Alumina supports is popular for the catalyst for its high thermal durability with a high surface area. Some other supports have been developed for improving SO_x durability as described later.

B. Improvement of Durability against Sulfur Poisoning

One of the big problems for NSR catalyst is SO_x poisoning. The storage material forms stable sulfates in lean conditions and loses NO_x adsorption

capability. To improve SO_x durability of NSR catalyst, a variety of approaches had been tried, such as additives, supports and substrate structure.

The effect of the addition of transition metal elemets to $Pt/Ba/Al_2O_3$ catalyst was investigated for improving SO_x durability (Yamazaki *et al.*, 2001, 2004). NO_x reducing activity of the catalyst was improved by some additives, and the highest activity was gained upon Fe-compound addition after aging test containing SO_2. However, the addition of a Cu-compound had a negative effect on the NSR catalysis. Figure 29 shows SO_x desorption performance of different Fe loading amount to $Pt/Ba/Al_2O_3$ exposed to an oxidizing atmosphere containing SO_2. This result indicates that the Fe-compound promotes the SO_2 desorption from the NSR catalyst. Figure 30 shows the $BaSO_4$ particle size on the $Pt/Ba/Al_2O_3$ varies against Fe loading. The $BaSO_4$ particle size of Fe-containing catalysts is far smaller than that of $Pt/Ba/Al_2O_3$, and the $BaSO_4$ particle was smaller with increasing the amount of Fe loading. These results indicate that Fe-compound inhibits the growth in size of $BaSO_4$ particles under oxidizing condition in the presence of SO_2. Therefore, the Fe-compound promotes the decomposition of $BaSO_4$ particles and the sulfur desorption when exposed to reducing conditions. The effect of Fe-compound addition on its TWC performance was also studied with $Pt/Ba/Al_2O_3$–CeO_2 catalyst to improve the durability against thermal deterioration. The catalyst with Fe-compounds showed a higher catalytic performance after thermal aging at 850°C. It was assumed that, Fe-compound addition suppressed CO poisoning on precious metal of the catalyst. Therefore, the Fe-compound plays two important roles; (1) acting as oxygen storage site more effectively, (2) weakening the CO self-poisoning under reducing conditions, probably by providing oxygen to CO from iron oxide and/or Fe in Pt–Fe alloy.

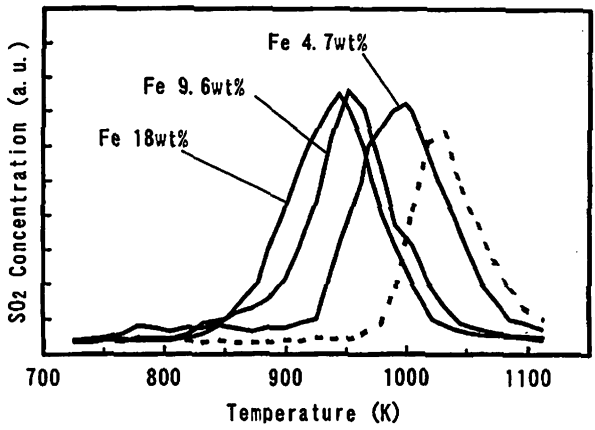

FIG. 29. SO_2 desorption profile of TPD measurement on the $PtBa/Al_2O_3$ with Fe-compounds exposed to a simulated oxidizing condition containing SO_2.

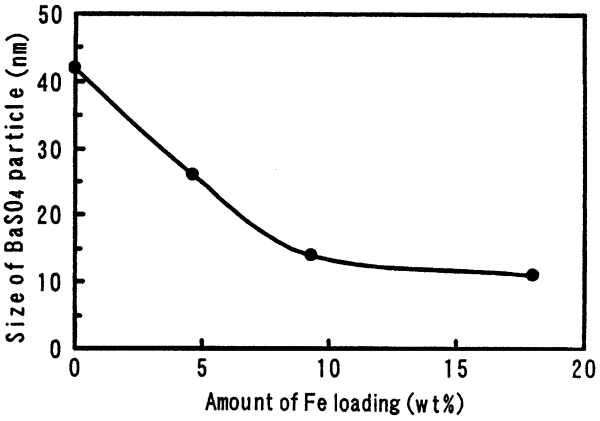

FIG. 30. Effect of Fe loading to $BaSO_4$ particle size on $Pt/Ba/Al_2O_3$ catalysts.

H_2 has a great potential for reducing sulfates on the catalyst as described earlier. Rh loaded on ZrO_2 was found to provide the high catalytic activity for H_2 formation by steam reforming reaction (Duprez, 2006). The most effective way to sustain the reaction of H_2 with sulfate is probably to produce H_2 in the proximity of barium sulfate. Figure 31(a) shows the effect of Rh/ZrO_2 addition to the NSR catalyst after an engine test of sulfur poisoning. Sulfur was easier to desorb from the catalyst with Rh/ZrO_2 in reducing condition. Figure 31(b) illustrates a scheme of Rh/ZrO_2 addition to Pt/Ba/alumina catalyst. H_2 is produced on Rh/ZrO_2 by steam reforming reaction, then react and decompose sulfate in reducing condition, resulting in the enhancement SO_x removal on the catalyst.

As for support material, TiO_2 addition to the NSR catalysts leads to improve the durabily of the catalyst against sulfur poisoning (Duprez, 2006). TiO_2 is an acidic material, and sulfates on TiO_2 are less stable than that on alumina. Therefore, TiO_2 particle dispersed in the alumina-based catalyst promotes the decomposition and removal of sulfates in the reducing condition. The promotion for SO_x desorption is much more facilitated by smaller particle size of TiO_2, which could be dispersed highly in the catalyst.

ZrO_2 is also effective for a support on K-compounds for high temperature use, for K-compound is apt to interact with alumina and TiO_2 to loose its NO_x storage ability. Recently, ZrO_2–TiO_2 mixed oxide as a support for K-compounds was found to improve the NO_x removal activity (Takahashi *et al.*, in press). Figure 32 shows NO_x storage activity after aging with SO_2 as a function of ZrO_2 content using simulated exhaust gases. A relative high ability above 500°C was obtained with 60–80 wt% ZrO_2 content, particularly at 70%. Figure 33 shows the state of potassium after the aging test with SO_2 of the three catalyst, TiO_2, ZrO_2 and ZT70 (70% ZrO_2–30% TiO_2) as a support. The results indicate that the catalyst with ZT70 retained the highest amount of remaining active potassium,

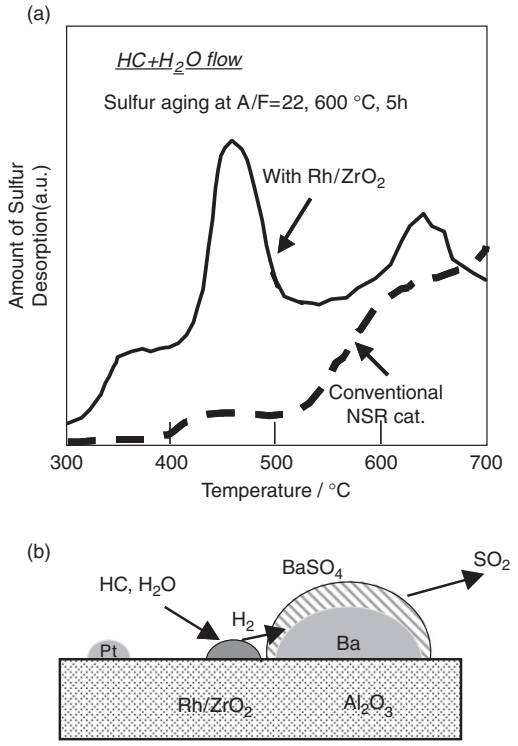

FIG. 31. (a) Effect of Rh/ZrO_2 addition for sulfur desorption. (b) Schematic effect of Rh/ZrO_2 addition to NSR catalyst for sulfur desorption.

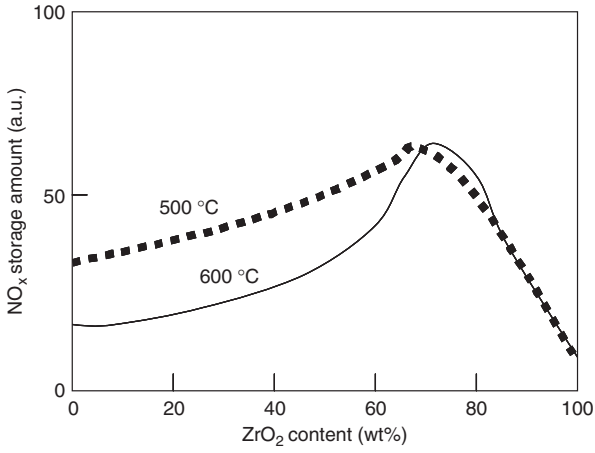

FIG. 32. NO_x removal performance of several ZrO_2–TiO_2 catalysts after the sulfur aging test.

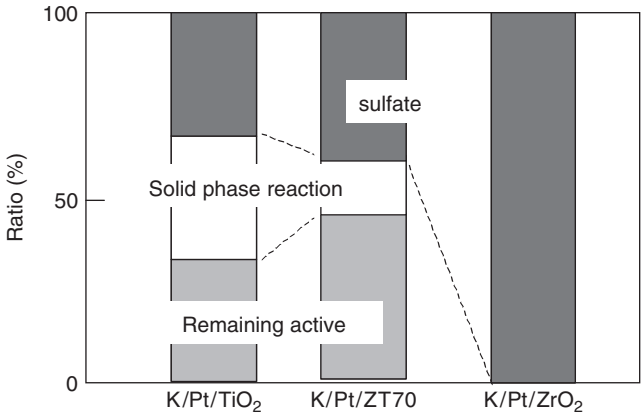

FIG. 33. The state of potassium over the sulfur-aged catalysts.

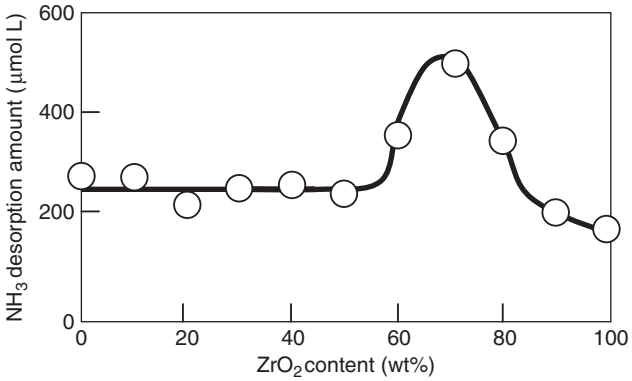

FIG. 34. NH_3 desorption amount for several ZrO_2–TiO_2 oxides.

which was neither the formed-sulfate nor the solid-phase-reacted potassium. The acidity of support is an important factor regarding the SO_x tolerance of the NSR catalyst. The catalyst containing ZT70 was verified to have the highest acid amount by NH_3 Temperature Programmed Desorption (TPD) measurement (Fig. 34), and was supposed to be the best against SO_x poisoning among the ZrO_2–TiO_2 supports. Furthermore, nano-level composite between alumina and ZT was found to improve thermal durability of the ZT support (Fig. 35) (Imagawa *et al.*). Figure 35b illustrates the scheme of this material (AZT). At high temperature, ZT particle is easy to agglomerate each other. As the result, the surface area of the ZT decreases, causing degradation of NSR activity. Alumina for a stable substance inhibits the sintering of ZT particle in high temperature region. NO_x storage amount of the catalyst containing AZT was higher than that of the catalyst of ZT after SO_x aging test as shown at Fig. 36.

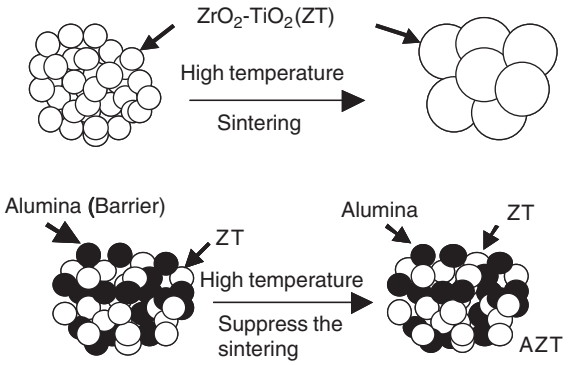

(a) Scheme of the AZT concept

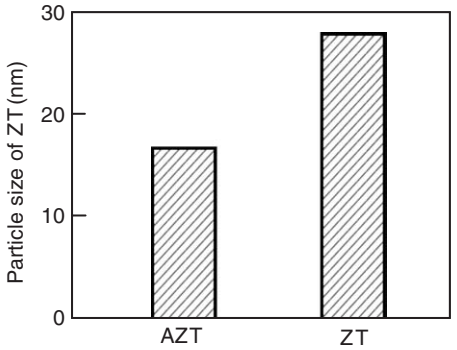

(b) Particle size of ZT after thermal ageing test at 1273 K.

FIG. 35. (a) The concept of complex oxide of zirconia, titania and alumina (AZT) and (b) its effect on thermal durability after thermal aging test at 1,000°C.

One of the rate-determining processes on the whole NSR reaction is a diffusion of NO_x and SO_x in the catalyst. The thickness of catalyst component coat on the substrate also affects the NSR activity. The conventional catalyst converters have square-shaped cells for the substrate of catalyst support. The thickness of coating usually becomes a much greater thickness at the corner (Fig 37a). However, the thickness of coatings with a hexagonal cell substrate (Fig. 37b) is almost the same compared to that on the square cell substrate. From the results of engine test, SO_x desorption of the catalyst was great improved with the hexagonal-type cell substrate, and NSR activity on the catalyst after durability test was also superior to the conventional catalyst with the square cell substrate.

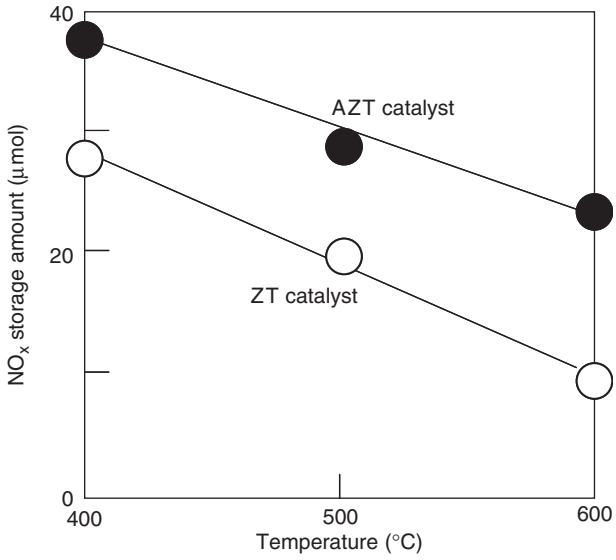

FIG. 36. The NO_x storage performance of ZT catalyst and AZT catalyst after sulfur-poisoning test.

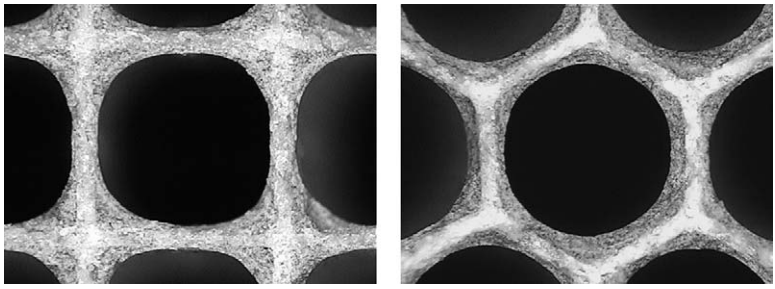

FIG. 37. Photographs of wash-coat layer on monolithic substrate with square cells (left) and hexagonal cells (right) (see Plate 1 in Color Plate Section at the end of this book).

C. COMBINATION OF CATALYSTS

Among the many published reports on the applications of the catalytic system, the addition of an oxidation catalyst upstream of an NSR catalyst improved NO_x storage activity through promoting NO_2 formation under oxidative atmosphere. As described earlier, coexistence of reducing gas such as HC, CO is reduced NO_2 into NO even in oxidizing atmosphere. Therefore, oxidation catalyst placed in front of NSR catalyst is necessary.

Through investigating the effect from the combination of several types of catalysts, it was found that a particular catalyst combination, Pd/Al_2O_3, NSR catalyst and Cu/zeolite in turn, showed a high NO_x reduction activity under oxidative atmosphere with periodic deep rich operation (Shinjoh *et al.*, in press). NO_x conversion with catalyst combinations of Pd/Al_2O_3 + NSR catalyst and Pd/Al_2O_3 + NSR catalyst + Cu/zeolite were measured in simulated automotive exhaust gases with periodically fluctuation between oxidative and reductive atmospheres. Comparing NO_x conversions on them under the oxidative atmosphere in Fig. 38, the effect of Cu/zeolite addition for improving NO_x conversion was remarkably indicated between 130 and 310°C. From the evolution patterns of gases, NO_x, NH_3 and HC, at 310°C on Pd/alumina + NSR catalyst and Pd/alumina + NSR catalyst + Cu/zeolite in the measurement (Fig. 39), it was suggested that NH_3 and HC were adsorbed under the reductive atmosphere and reacted with NO_x under the oxidative atmosphere on Cu/zeolite. Figure 40 shows NO_x reduction activities on Cu/zeolite with the pre-adsorbed NH_3 or C_3H_6 under oxidative atmosphere. These results indicated that the adsorbed NH_3 selectively reacted with NO_x at equal molar ratio, while the adsorbed C_3H_6 reacted with both NO_x and O_2. From these results, the high NO_x reduction activity with this combination of catalysts could be elucidated by the following reaction mechanism (Fig. 41): Pd catalyst upstream of the NSR catalyst improved NO_x storage ability by enhancing NO_2 formation under oxidative atmosphere, the stored NO_x was apt to be reduced to NH_3 on the NSR catalyst. The generated NH_3 was adsorbed on Cu/zeolite downstream of

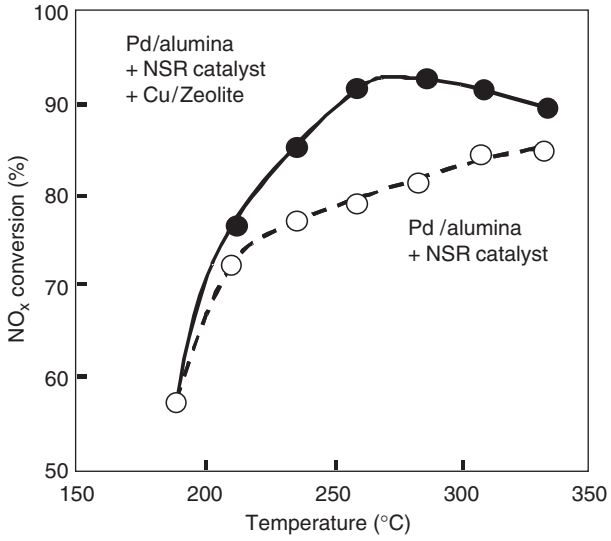

FIG. 38. NO_x reduction activity in cycled feed stream.

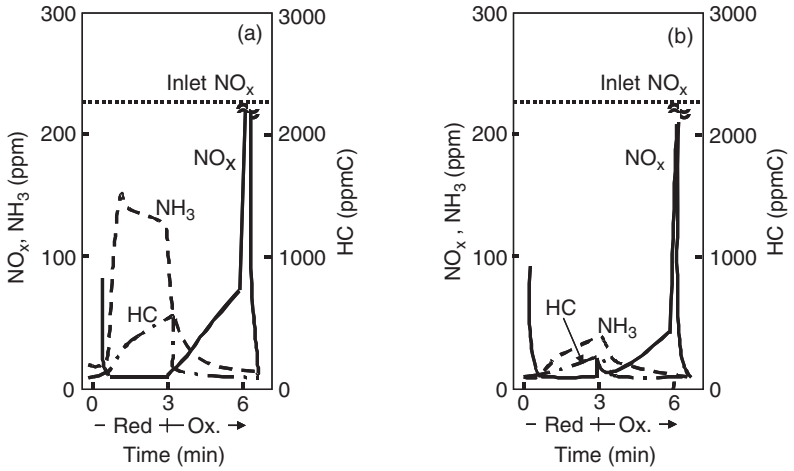

FIG. 39. Evolution pattern of several gases in cycled feed stream at 310°C. (a) Pd/Al_2O_3 + NSR catalyst and (b) Pd/Al_2O_3 + NSR catalyst + Cu/Zeolite.

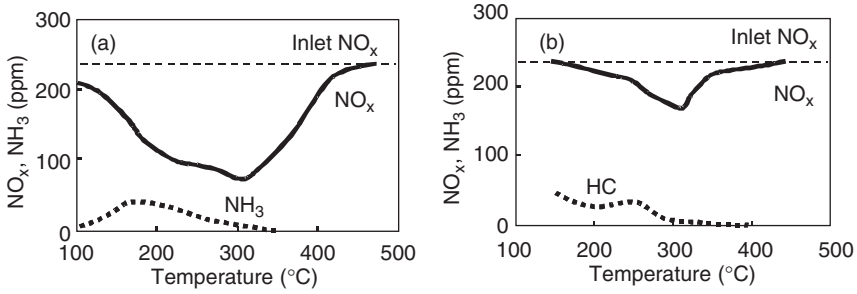

FIG. 40. NO_x reduction activity with pre-adsorbed NH_3 or C_3H_6 on Cu/Zeolite. After saturating the adsorbtion of a reductant: (a) NH_3 and (b) C_3H_6, on Cu/Zeolite, NO_x reduction activity was measured with increasing temperatures at 20°C/min under the oxidizing atmosphere.

the NSR catalyst under the reductive atmosphere, and easily reacted with NO_x on the Cu/zeolite under the subsequent oxidative atmosphere.

The NSR technology has been also applied to diesel engines, and is most reliable and attractive method for lean-burn combustion vehicles. Diesel particulate-NOx reduction system (DPNR) method is used to realize the simultaneous and continuous reduction of particulate and NO_x is also recommended. This catalyst system is DPF combined with NSR catalyst. Soot on catalyst is removed during NO_x reduction by occasional rich engine modification. Many other catalyst systems with NSR catalyst have been also developed. With decreasing S content in fuel and successive development of

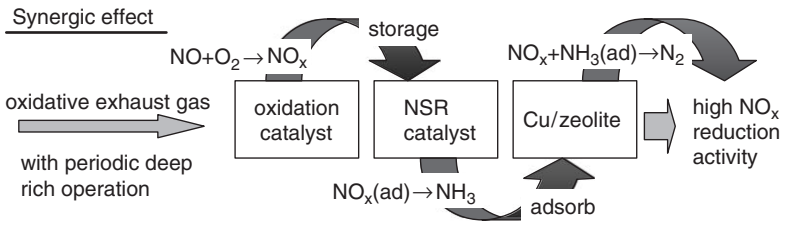

FIG. 41. Schematic concept of the synergy effect of the catalyst combination.

catalyst will lead to the worldwide prevailing of this kind of catalyst. We expect for great progress and big improvements in cleaning the exhaust gases, as well as the fuel economy by using these techniques in the near future.

VII. Conclusions

This chapter reviews the recent progress of research on the dynamic behavior and characterization of automobile catalysts mainly done in our laboratory. Basically, automobile catalysts are used under the non-steady condition in which a gas concentration, a gas flow rate and a temperature fluctuate with a car-driving mode. Therefore, it is very important for developing automobile catalysts to clarify the mechanism of their dynamic behavior and characterize the structure and state of materials under dynamic conditions. Four topics on the dynamic phenomena for TWC and NSR catalysts were described in this chapter.

(1) Oxygen storage and release in TWCs

The precise local structure around Ce and Zr atoms of CeO_2–ZrO_2 mixed oxide (CZ) was investigated to clarify their effects on OSC. The amount of OSC per Ce atom of R–CZ (prepared by the calcination of M–CZ with graphite at 1,200°C under a reducing atmosphere) is much higher than that of S–CZ (prepared by an attrition milling process of CeO_2 powder with ZrO_2 spheres in ethanol) and M–CZ (prepared by the hydrolysis of an aqueous solution of $ZrO(NO_3)_2$ with ammonia on CeO_2 powder), and is close to the theoretical value of 0.25, which means almost all of the quadruvalent Ce are reduced into trivalent Ce. The oxygen mobility in CZ materials is of similar magnitude. The regular arrangement of Ce and Zr atoms in R–CZ probably eases the release of oxygen.

A new material ACZ for a TWC with high thermal stability is developed based on a novel concept, i.e. the diffusion barrier concept. Diffusion

barrier layers of Al_2O_3 are built up between CZ particles to inhibit the coagulation or grain growth of CZ.

(2) Sintering of PGM

The X-ray absorption analysis of Pt catalysts suggests that the Pt-oxide-support interaction inhibits the sintering of Pt particles and the sintering inhibition effect on Pt can be controlled by the electron density of oxygen in the support through the Pt–O–Ce bond.

The real-time observation of sintered Pt on CZ materials by *in situ* time-resolved Turbo-XAS demonstrates the re-dispersion of Pt particles. The Pt particle size of the aged catalyst decrease from 7 to 5 nm after 60 s and then to 3 nm after 1,000 s under the alternating flow of reducing and oxidizing gases at 600°C.

These results suggest that the sintering and re-dispersion of Pt is highly affected by the characteristics of the surface oxygen of supports.

(3) NSR catalyst and reaction mechanism

Four reaction steps, (a) to (d), are the main routes in the NSR reaction and the most difficult problem to be solved for the NSR catalyst is the deactivation caused by sulfur poisoning. The course of improvement of the NSR catalyst is proposed. (a) NO oxidation to NO_2 (oxidizing condition): both NO oxidation to NO_2 and the removal of the residual reducing agents from exhaust gas are necessary for improving the NO_x storage performance at low temperature, (b) NO_x storage in basic materials (oxidizing condition): amorphous barium carbonate shows relatively low thermal stability and possesses high reactivity for NO_x storage, (c) NO_x release from the basic material (reducing condition): accelerated by Pt coexistence with promoting the reactions and (d) NO_x reduction to N_2 (reducing condition): H_2 generated by water gas shift reaction is quite effective for the reduction.

BaO within a few nanometers around the Pt can work as NO_x storage material in the reaction containing SO_2. Also, the smaller the sulfate particle size in the aged catalyst is, the easier its decomposition.

(4) Improve NSR catalyst and system

The NO_x storage amount has a good correlation with the electron negativity of storage materials. Barium compounds have been used widely for high NO_x storage ability and its thermal stability. Potassium compounds are another component with a significant benefit at higher temperatures.

The addition of a Fe-compound inhibits the growth in size of $BaSO_4$ particles under oxidizing conditions in the presence of SO_2, and then the Fe-compound promotes the decomposition of $BaSO_4$ particles and the sulfur desorption when exposed to reducing conditions. Also, the catalyst with Fe-compounds shows a higher catalytic performance after thermal aging at 850°C. This suggests that the addition of a Fe-compound suppresses CO poisoning on precious metal of the catalyst. That is, the

Fe-compound plays two important roles: (1) acting as oxygen storage site more effectively, (2) weakening the CO self-poisoning under reducing conditions, probably by providing oxygen to CO from iron oxide and/or Fe in Pt–Fe alloy.

Rh/ZrO_2 has the high catalytic activity for H_2 formation by steam reforming reaction. In the NSR catalyst contained Rh/ZrO_2, H_2 is produced on Rh/ZrO_2 by steam reforming reaction, and then sulfates are decomposed in reducing condition, resulting in the enhancement of SO_x removal from sulfur-poisoned catalyst.

TiO_2 addition to the NSR catalysts leads to an improvement of SO_x resistance of the catalyst. TiO_2 is an acidic material, and sulfates on TiO_2 are less stable than that on alumina. Hence, TiO_2 promotes the decomposition and removal of sulfates in reducing conditions. Also, ZrO_2–TiO_2 mixed oxide as a support for K-compounds improves the NO_x removal activity.

One of the rate-determining processes on the whole NSR reaction is a diffusion of NO_x and SO_x in the catalyst. The thickness of coatings with a hexagonal cell substrate is almost uniform, therefore, SO_x desorption of the catalyst is greatly improved with the hexagonal cell substrate compared to that on the conventional square cell.

An oxidation catalyst placed upstream of an NSR catalyst improves NO_x storage activity through promoting NO_2 formation under oxidative atmosphere and oxidizes coexisting reducing gas such as HC, CO which reduces NO_2 into NO even in oxidizing atmosphere. The NSR technology is also applied to diesel engines. DPNR which combines a DPF with an NSR catalyst realizes the simultaneous reduction of particulate and NO_x. Soot on catalyst is removed during the NO_x reduction process by an occasional rich engine operation.

We have a dream of realizing a car which purifies the air of the earth through its driving. We will be improving an automobile catalyst on and on as described in this chapter: oxygen storage capacity, NSR ability, etc. In addition, we would be making efforts to clarify the nature of catalysis in automobile catalysts, i.e. electronic interaction between PGM, supports and exhaust gases, dynamic observations of an electronic state of catalysts and reaction kinetics, etc. for realizing our dream.

REFERENCES

Burch, R., and Watling, T. C. *Catal. Lett.* **37**, 51 (1996).

Cant, N. W., Liu, I. O. Y., and Patterson, M. J. *J. Catal.* **243**, 309 (2006).

Dong, F., Suda, A., Tanabe, T., Nagai, Y., Sobukawa, H., Shinjoh, H., Sugiura, M., Descorme, C., and Duprez, D. *Catal. Today* **90**, 223 (2004a).

Dong, F., Suda, A., Tanabe, T., Nagai, Y., Sobukawa, H., Shinjoh, H., Sugiura, M., Descorme, C., and Duprez, D. *Catal. Today* **93**, 827 (2004b).
Duprez, D. *Catal.Today* **112**, 17 (2006).
Epling, W. S., Campbell, L. E., Yezerets, A., Currier, N. W., and Parks, J. E. *Catal. Rev.* **46**, 163 (2004).
Fiedorow, R. M. J., Chahar, B. S., and Wanke, S. E. *J. Catal.* **51**, 193 (1978).
Forzatti, P. *Appl.Catal. A* **222**, 221 (2001).
Fridell, E., Persson, H., Westerberg, B., Oksson, L., and Skoglundh, M. *Catal. Lett.* **66**, 71 (2000).
Fridell, E., Skoglundh, M., Westerberg, B., Johansson, S., and Smedler, G. *J. Catal.* **183**, 196 (1999).
Gandhi, H. S., Piken, A. G., Shelef, M., and Delesh, R. G., *SAE Technical Paper 760201* (1976).
Greegor, R. B., and Lytle, F. W. *J. Catal.* **63**, 476 (1980).
Hamada, H., Kintaichi, Y., Sasaki, M., Ito, T., and Tabata, M. *Appl. Catal.* **64**, L1 (1990).
Harris, P. J. F. *J. Catal.* **97**, 527 (1986).
Held, W., and Konig, A., SAE Technical Paper 900496 (1990).
Imagawa, H., Tanaka, T., Takahashi, N., Matsunaga, S., and Shinjoh, H., TOCAT5, PI-430, Tokyo, Japan (2006).
Iwamoto, M., Yahiro, H., Yu-u, Y., Shundo, S., and Mizuno, N. *Shokubai* **32**, 430 (1990).
Iwamoto, M., Yokoo, S., Sakai, K., and Kagawa, S. *J. Chem. Soc. Faraday Trans. 1* **77**, 1629 (1981).
Johnson, T. V. *Soc. Automot. Eng.* **SP-1581**, 23 (2001).
Kanazawa, T., Suzuki, J., Takada, T., Suzuki, T., Morikawa, A., Suda, A., Sobukawa H., and Sugiura, M., SAE Technical Paper 2003-01-0811 (2003).
Kato, K., Kihara, T., Asamuna, T., Gotoh, M., and Shibagaki, S. *Toyota Tech. Rev.* **44**, 2 (1994).
Konsolakis, M., and Tentekakis, I. V. *Appl. Catal. B* **29**, 103 (2001).
Kummer, J. K. *Prog. Energy Combust. Sci.* **6**, 177 (1980).
Lietti, L., Forzatti, P., Nova, I., and Tronconi, E. *J. Catal.* **204**, 175 (2001).
Matsumoto, S. *Catal. Today* **90**, 183 (2004).
Matsumoto, S., Miyoshi, N., Kanazawa, T., Kimura, M., and Ozawa, M., *in* "Catal. Sci. Technol." (S. Yoshida, N. Takezawa, and T. Ono Eds.), Vol. 1, p. 335. Kodansha, Tokyo (1991).
Miyoshi, N., Matsumoto, S., Ozawa, M., and Kimura, M., SAE Technical Paper 891970 (1989).
Muraki, H., Sobukawa, H., and Fujitani, Y. *Nippon Kagaku Kaishi* **176**, (1985).
Nagai, Y., Hirabayashi, T., Dohmae, K., Takagi, N., Minami, T., Shinjoh, H., and Matsumoto, S. *J. Catal.* **242**, 103 (2006).
Nagai, Y., Takagi, N., Ikeda, Y., Dohmae, K., Tanabe, T., Pascarelli, S., Guilera, G., Newton, M., Shinjoh, H., and Matsumoto, S., PI-439, TOCAT5, 2006, Tokyo, Japan.
Nagai, Y., Yamamoto, T., Tanaka, T., Yoshida, S., Nonaka, T., Okamoto, T., Suda, A., and Sugiura, M. *J. Synchrotoron Rad.* **8**, 616 (2001).
Nagai, Y., Yamamoto, T., Tanaka, T., Yoshida, S., Nonaka, T., Okamoto, T., Suda, A., and Sugiura, M. *Catal. Today* **74**, 225 (2002).
Nishihata, Y., Mizuki, J., Akao, T., Tanaka, H., Uenishi, M., Kimura, M., Okamoto, T., and Hamada, N. *Nature* **418**, 164 (2002).
Ozawa, M., Kimura, M., and Isogai, A. *J. Mater. Sci.* **26**, 4818 (1991).
Ozawa, M., Kimura, M., and Isogai, A. *J. Alloys Comp.* **193**, 73 (1993).
Piacentini, M., Maciejewski, M., and Baiker, A. *Appl. Catal. B* **59**, 187 (2005).
Sakamoto, Y., Okumura, K., Kizaki, Y., Matsumnaga, S., Takahashi, N., and Shinjoh, H. *J. Catal.* **238**, 361 (2006).
Shinjoh, H., Muraki, H., and Fujitani, Y., *Stu. Surf. Sci. Catal.* **30**, 187, Elsevier, Amsterdam (1987).
Shinjoh, H., Muraki, H., and Fujitani, Y. *Appl.Catal.* **49**, 195 (1989).
Shinjoh, H., Muraki, H., and Fujitani, Y., Proceedings of the 2nd International Symposium (CAPOC2), Brussels, September 10–13 (1990).
Shinjoh, H., Takahashi, N., and Yokota, K., *Topics Catal*. (in press).

Suda, A., Kandori, T., Sobukawa, H., and Sugiura, M. *J. Ceram. Soc. Jpn.* **108**, 473 (2000).
Suda, A., Sobukawa, H., Suzuki, T., Kandori, K., Ukyo, Y., and Sugiura, M. *J. Ceram. Soc. Jpn.* **109**, 177 (2001).
Suda, A., Ukyo, Y., Sobukawa, H., and Sugiura, M. *J. Ceram. Soc. Jpn.* **110**, 126 (2002).
Takahashi, N., Shinjoh, H., Iijima, T., Suzuki, T., Yamazaki, K., Yokota, K., Suzuki, H., Miyoshi, N., Matsumoto, S., Tanizawa, T., Tanaka, T., Tateishi, S., and Kasahara, K. *Catal. Today* **27**, 63 (1996).
Takahashi, N., Suda, A., Hachisuka, I., Sugiura, M., Sobukawa, H., and Shinjoh, H., *Appl. Catal. B* (in press).
Takahashi, N., Yamazaki, K., Sobukawa, H., and Shinjoh, H. *J. Chem. Eng. Jpn.* **39**, 437 (2006).
Takahashi, N., Yamazaki, K., Sobukawa, H., and Shinjoh, H., *Appl. Catal. B* (in press).
Toops, T. J., Smith, D. B., and Partridge, W. P. *Catal. Today* **114**, 112 (2006).
Xue, E., Seshan, K., and Roth, J. R. H. *Appl. Catal. B* **11**, 65 (1996).
Yamazaki, K., Suzuki, T., Takahashi, N., Yokota, K., and Sugiura, M. *Appl. Catal. B* **30**, 459 (2001).
Yamazaki, K., Takahashi, N., Shinjoh, H., and Sugiura, M. *Appl. Catal. B* **53**, 1 (2004).
Yokota, K., Muraki, H., and Fujitani, Y., SAE Technical Paper 850129 (1985).
Yoshida, H., Nonoyama, S., Yazawa, Y., and Hattori, T. *Phy. Scr. T* **115**, 813 (2005).

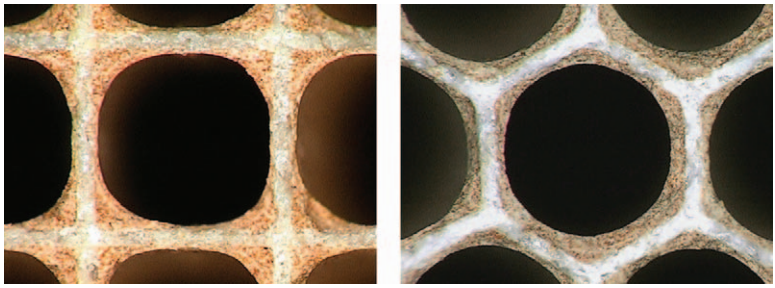

PLATE 1. Photographs of wash-coat layer on monolithic substrate with square cells (left) and hexagonal cells (right) (for Black and White version, see page 39).